

Air-density-dependent model for analysis of air heating associated with streamers, leaders, and transient luminous events

Jeremy A. Rioussset,¹ Victor P. Pasko,¹ and Anne Bourdon²

Received 10 July 2010; revised 31 August 2010; accepted 23 September 2010; published 18 December 2010.

[1] Blue and gigantic jets are transient luminous events in the middle atmosphere that form when conventional lightning leaders escape upward from the thundercloud. The conditions in the Earth's atmosphere (i.e., air density, reduced electric field, etc.) leading to conversion of hot leader channels driven by thermal ionization near cloud tops to nonthermal streamer forms observed at higher altitudes are not understood at present. This paper presents a formulation of a streamer-to-spark transition model that allows studies of gas dynamics and chemical kinetics involved in heating of air in streamer channels for a given air density N under assumption of constant applied electric field E . The model accounts for the dynamic expansion of the heated air in the streamer channel and resultant effects of E/N variations on plasma kinetics, the vibrational excitation of nitrogen molecules $N_2(v)$, effects of gains in electron energy in collisions with $N_2(v)$, and associative ionization processes involving $N_2(A^3\Sigma_u^+)$ and $N_2(a^1\Sigma_u^-)$ species. The results are in excellent agreement with available experimental data at ground and near-ground air pressures and demonstrate that for the air densities corresponding to 0–70 km altitudes the kinetic effects lead to a significant acceleration of the heating, with effective heating times scaling closer to $1/N$ than to $1/N^2$ predicted on the basis of similarity laws for Joule heating. This acceleration is attributed to a strong reduction in electron losses due to three-body attachment and electron-ion recombination processes with reduction of air pressure.

Citation: Rioussset, J. A., V. P. Pasko, and A. Bourdon (2010), Air-density-dependent model for analysis of air heating associated with streamers, leaders, and transient luminous events, *J. Geophys. Res.*, 115, A12321, doi:10.1029/2010JA015918.

1. Introduction

[2] The observed phenomenology of a subset of the recently recorded transient luminous events (TLEs) in the middle atmosphere, which originate from thundercloud tops [e.g., *Wescott et al.*, 2001; *Pasko et al.*, 2002; *Su et al.*, 2003; *Krehbiel et al.*, 2008; *Cummer et al.*, 2009; *Rioussset et al.*, 2010], indicate that these events, so-called blue and gigantic jets, may be related to conventional lightning leader processes as initially proposed by *Petrov and Petrova* [1999]. *Wescott et al.* [2001] have reported a 2 min time exposure color photograph of a jet event taken from St. Denis, Réunion Island in the Indian Ocean. The corresponding inverted black and white image from *Wescott et al.* [2001] is reproduced in Figure 1a and shows details of faint streamers diverging from the main body of the jet. Figure 1b shows an image obtained by averaging of 48 video fields extracted from the 24 frame video sequence corresponding to a similar event observed in Puerto Rico [*Pasko et al.*, 2002]. The image in Figure 1b effectively simulates how the observed event would look if

captured on a photograph with an exposure time exceeding the total duration of the event (~ 0.8 s). Figure 1b shows a very similar structure to Figure 1a in terms of faint streamers diverging at large angles from the main body of the jet. The original video sequence presented by *Pasko et al.* [2002] indicates that these streamers are formed at the initial stage of the jet development. Therefore, the streamer structure in Figure 1a was likely formed at the initial stage of that event development, similarly to the event reported by *Pasko et al.* [2002] (Figure 1b). Figure 1b shows a very bright channel at the bottom of the image (between altitudes of approximately 16 and 20 km). We interpret the appearance of this bright feature in both Figures 1a and 1b as the streamer-to-leader transition involving strong heating and thermalization usually associated with a leader phenomenon. This interpretation is supported by the original color photograph of *Wescott et al.* [2001], in which the lower portion of the event in Figure 1a has a bright white color. Therefore, these events are believed to be associated with significant heating of the air in the regions of atmosphere near the cloud tops through which they propagate [*Pasko and George*, 2002]. The small-scale filamentary structures in the upper parts of the observed jets, identical to those observed in another type of TLEs at higher altitudes called sprites [e.g., *Stenbaek-Nielsen et al.*, 2007, and references therein], can be associated with corona streamers. Such streamer coronas are expected to constitute an essential part of the streamer zone of the parent lightning

¹Communications and Space Sciences Laboratory, Department of Electrical Engineering, Pennsylvania State University, University Park, Pennsylvania, USA.

²Energetics and Combustion Laboratory, UPR CNRS 288, École Centrale Paris, Châtenay-Malabry, France.

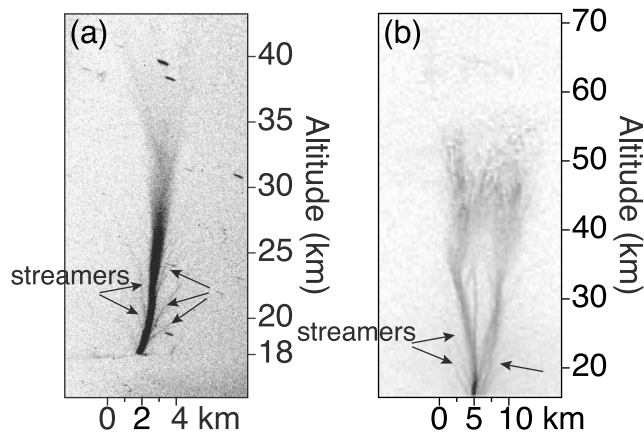


Figure 1. (a) A black and white image of a 2 min time exposure of a blue jet [Wescott et al., 2001]. (b) Processed image obtained by averaging of sequence of video fields from observations reported by Pasko et al. [2002] (<http://pasko.ee.psu.edu/Nature/>). Reprinted from Pasko and George [2002].

leader [e.g., Bazelyan and Raizer, 1998, pp. 204, 238, and 253] as hypothesized by Petrov and Petrova [1999].

[3] We note that air heating effects in sprite streamers also may be relevant to the recently discovered infrasound radiation from sprites [Farges et al., 2005; Liszka and Hobara, 2006; Pasko and Snively, 2007; Farges, 2009; Farges and Blanc, 2010; De Larquier, 2010].

[4] Recently, Krehbiel et al. [2008] discussed the charge imbalances in thunderstorms as a fundamental condition allowing propagation of leaders downward as cloud-to-ground lightning or upward as jet discharges. This work demonstrates that upward discharges are analogous to cloud-to-ground lightning and provides a unified view on how lightning escapes from a thundercloud. Krehbiel et al. [2008] note that in accordance with existing experimental evidence, the lightning initiation usually happens between adjacent charge regions of different polarity where the electric field is the highest. If the negative and positive charge centers are approximately equal in magnitude, then the bidirectional discharge propagates in the form of positive leaders inside of the negative charge region and in the form of negative leaders inside of the positive charge region [e.g., Rioussset et al., 2007]. In this situation, the leader system, which is assumed to be overall equipotential and neutral, remains at nearly zero potential [Rioussset et al., 2007]. Krehbiel et al. [2008] demonstrate that when the two charges are not balanced, the leader potential can be significantly shifted in the direction defined by the charge with dominant magnitude, and the propagation of the leader becomes essentially independent from the weaker charge center, allowing it to penetrate through the weaker charge center and to escape from the thundercloud. To further support the ideas advanced by Krehbiel et al. [2008], Rioussset et al. [2010] introduce a two-dimensional axisymmetric model of charge relaxation in the conducting atmosphere and apply this model in conjunction with the three-dimensional lightning model proposed by Rioussset et al. [2007] to illustrate how blue and gigantic jet discharges are produced above cloud tops. The results of Krehbiel et al. [2008] and Rioussset et al. [2010] provide a quantitative picture of how the lightning leader can escape the

cloud upward and serve as the initiation of blue and gigantic jets. The exact details of the transition from the hot leader channel near the cloud top to the streamer-dominated forms observed in jets at high altitude are not understood at present. One of the goals of the present paper is to make a first quantitative step in understanding the elementary scaling of air heating associated with streamers and leaders as a function of the ambient air density in the range corresponding to altitudes of 0–70 km in the Earth atmosphere.

[5] After appropriate scaling with air density, the corona streamers observed in Figure 1 are fully analogous to those that initiate spark discharges in relatively short (several cm) gaps at near-ground pressure [Liu et al., 2009, and references therein] and that are known to constitute building blocks of streamer zones of conventional lightning leaders and leaders in long gaps in laboratory experiments [e.g., Gallimberti, 1979; Bazelyan and Raizer, 1998, pp. 204, 238, and 253; Gallimberti et al., 2002]. The scaling of the parameters of streamer discharges as a function of air density N (e.g., streamer radius $r_s \propto 1/N$, streamer electron density $n_{e,s} \propto N^2$, and dielectric relaxation time in the streamer body $\tau_s \propto 1/N$) has been discussed for sprite discharges in the middle atmosphere and can be readily used to establish a similarity law for the Joule heating timescale (i.e., its scaling with neutral density) [Pasko et al., 1998]. Indeed, assuming for simplicity of presentation that air density N , streamer electron density n_e and the electric field in the streamer channel \vec{E} remain constant, and that all Joule energy is transferred directly to heating of the gas, one can write an equation for the air temperature T_g in the form

$$\frac{dNk_B T_g}{dt} = (\gamma - 1) \vec{J} \cdot \vec{E}, \quad (1)$$

where $\vec{J} = q_e n_e \mu_e \vec{E}$ is the current density, q_e is electron charge, γ is the specific heat ratio and μ_e is the electron mobility. The scaling of streamer electron density with air density N is defined with respect to ground value N_0 as $n_e = n_{e,0} N^2/N_0^2$, where $n_{e,0}$ is the streamer electron density at the ground level. Other physical quantities can be expressed in similar form as $\mu_e = \mu_{e,0} N_0/N$ and $E = E_0 N/N_0$ [e.g., Pasko et al., 1998]. Having substituted these expressions in equation (1) one can represent time variation of air temperature T_g in the form

$$\frac{dT_g}{d(tN^2/N_0^2)} = \frac{(\gamma - 1)q_e n_{e,0}\mu_{e,0}E_0^2}{k_B} \quad (2)$$

that directly indicates that for reduced air density $N < N_0$ it takes a factor of N_0^2/N^2 longer time to produce the same increment in gas temperature T_g (e.g., 5000 K, see further discussion below). Therefore, the general scaling of the Joule heating timescale in the streamer channels as a function of air density is $\tau_h \propto 1/N^2$ [e.g., Achat et al., 1992; Tardiveau et al., 2001; Pasko, 2006]. Therefore, it is generally expected that the heating processes and resulting streamer-to-spark transition should be delayed with a reduction of air pressure (i.e., at higher altitudes in the Earth atmosphere), and it should be possible to define a set of specific conditions (i.e., altitude range, reduced electric field E/N , etc.) in the Earth atmosphere for which the transition becomes impossible. The present work represents a first step toward the modeling of the streamer-to-leader transition at various altitudes, which is

required to define these conditions. This first step is made necessary by the complexity of the problem. In particular, the heating of the streamer channel depends not only on the Joule heating but also on the relaxation of vibrationally excited N_2 molecules, on the complicated kinetics of electron detachment from negative ions, on the gas dynamics expansion of the channel, and on other factors as discussed below in this paper, and a simple similarity law for heating time-scale cannot be simply deduced from the similarity laws for streamers.

[6] Unlike the neutral gas density N , the pressure p is easily measured, and, therefore, commonly used for reference in experimental studies on the streamer-to-spark transition [e.g., *Achat et al.*, 1992; *Larsson*, 1998]. During the initial stages of the heating, the gas temperature T_g can be considered as constant so that p becomes equivalent to N , with their relationship obeying the classical law of perfect gases, $p = Nk_B T_g$, where k_B is the Boltzmann constant. When thermal gas expansion effects are accounted for, it is important to use the reduced electric field E/N , instead of E/p [e.g., *Tardiveau et al.*, 2001]. Consequently, in the present paper, we use reduced parameters as functions of the neutral gas density N similar to that used in other experimental [*Tardiveau et al.*, 2001] and theoretical [e.g., *Naidis*, 2005; *Popov*, 2009] works. In this work, we investigate the similarity law of heating timescale in the streamer-to-spark transition, i.e., its scaling with neutral density. The model developed for the studies reported in this paper builds on previous theoretical modeling of streamer-to-spark transition, a review of which is given below. It also complements experimental investigations of the pressure effects on the development of electric discharges in small gaps by *Achat et al.* [1992] and *Tardiveau et al.* [2001].

[7] The earliest qualitative model description of a streamer-to-spark transition by *Marode* [1983, and references therein] focuses solely on a thermal transition (i.e., based on gas dynamics expansion of the channel leading to a reduction in the gas density and to an increase in E/N). Later studies either include chemical kinetic processes as an alternative or a companion mechanism to the thermal mechanism. *Mnatsakanyan and Naidis* [1991] discuss the foundations of the chemistry models of electrical discharges. The first comprehensive kinetics scheme of the nonequilibrium discharge in nitrogen-oxygen mixtures is reported by *Kossyi et al.* [1992]. Many subsequent models of streamer breakdown in short gaps involving chemical kinetics [e.g., *Aleksandrov et al.*, 1997, 1998, 2001; *Naidis*, 1999, 2005, 2008; *Popov*, 2001, 2003, 2009; *Flitti and Pancheshnyi*, 2009] benefit from the exhaustive list of reactions investigated in this pioneering work.

[8] The first models of plasma heating by *Aleksandrov et al.* [1997, 1998] were developed in the framework of breakdown (by streamer or leader channels) in long air gaps (>5–10 m). *Aleksandrov et al.* [1997] 0-D model accounts for the influence of the electric field and gas temperature on the ionization kinetics to study the response time of the leader parameters to a step change in the gas temperature. It does not account for vibrational-translational relaxation of vibrational energy of N_2 molecules, which was introduced by *Aleksandrov et al.* [1998], following the principles discussed by, e.g., *Mnatsakanyan and Naidis* [1985]. *Aleksandrov et al.* [1998] 1.5-D model accounts for the fact that the Joule

heating owing to the current flow in the channel is not solely used to increase the temperature of the background gas. Instead, only a small fraction of the Joule heating energy, denoted η_T , is used to heat the channel in the so-called “fast heating” process mainly associated with relaxation of electronically excited states of N_2 and O_2 molecules; a significant fraction η_V of the Joule energy is transferred to and stored in the vibrational energy levels of the nitrogen molecules. *Aleksandrov et al.* [1998] conclude that the rapid gas heating is associated with a conversion of the energy of the electronically excited molecular states into heat via quenching of the excited molecules.

[9] *Aleksandrov et al.* [1998] consider that the effect of hydrodynamic expansion of the streamer channel on the streamer-to-spark transition is negligible because of the fairly short time of the channel formation. *Naidis* [1999] employs a similar model in 0-D involving 14 species including electrons, positive and negative ions, and excited radicals to propose two possible origins of the increase in plasma conductivity leading to the spark formation during streamer-to-spark transition [*Naidis*, 1999, 2005, and references therein]. The first one is a thermal mechanism, which leads to lowering of the gas number density N inside the channel due to the expansion of the heated gas [*Marode et al.*, 1979; *Marode*, 1983; *Bastien and Marode*, 1985]. As already noted above, this process leads to the growth of the mean reduced field E/N and, therefore, to an increase in the ionization rate. The second one is a kinetic mechanism related to the accumulation of active particles (radicals and excited molecules) changing the balance between the rates of generation and loss of electrons due to the acceleration of the detachment, stepwise and associative ionization [e.g., *Aleksandrov et al.*, 1998]. Both of these factors act simultaneously, but for practical analysis, it is possible to identify different parameter regimes when only one of these factors dominates [*Naidis*, 2005].

[10] A model by *Flitti and Pancheshnyi* [2009] employs 44 species participating in about 430 reactions to study the gas heating in fast-pulsed discharges in N_2 - O_2 mixtures. This work pays particular attention to the estimation of the fractions η_T and η_V , which are obtained with the BOLSIG+ solver of the Boltzmann equation for electrons in weakly ionized gases [*Hagelaar and Pitchford*, 2005]. Using this model, *Flitti and Pancheshnyi* [2009] show that higher electron density, electric field or partial pressure of oxygen leads to a faster gas heating, but that the heating rate associated with excitation of vibrational and electronic degrees of freedom is almost independent of the value of the applied electric field, in the range of fields studied. These authors also do not detect significant pressure dependence of the η_T and η_V parameters, in agreement with the results presented by *Popov* [2001].

[11] The investigation of the effects of the channel expansion discussed by *Naidis* [1999] requires suitable modeling of the gas dynamics of the plasma channel, and so a spatial dimension of the discharge needs to be introduced. Under the assumptions of a constant, uniform field along the channel axis, and of an axial symmetry of the discharge, one-dimensional time varying simulations of the streamer-to-spark transition have been shown to adequately model the heating of the channel [e.g., *Naidis*, 2005]. The 1-D axisymmetric, axially invariant model of the streamer-to-spark transition by *Aleksandrov et al.* [2001] adopts a 1-D

time-dependent hydrodynamic model under the isobaric approximation coupled to a 0-D kinetics scheme. *Aleksandrov et al.* [2001] employ a time- and space-dependent heat equation and a time-dependent homogeneous electron-density balance equation and suggest that kinetic mechanisms prevail over thermal processes (i.e., processes related to gas dynamic expansion). *Popov* [2001] developed a similar model involving a 0-D kinetics scheme coupled to 1-D time- and space-dependent system of equations comprising the equations of conservation of energy and electron number density (n_e) under the assumption of a constant neutral density. The salient difference between the equations of balance of electrons as it appears in the *Naidis* [1999] and *Popov* [2001] models resides in the spatial dependence of n_e that is described in the latter by the ambipolar diffusion equation. The model is used to investigate the contribution of the vibrational-translational relaxation to the rapid gas heating in nitrogen-oxygen mixtures and concludes that the contribution of the vibrational-translational relaxation reactions to the total rate of gas heating should increase with gas pressure because of the increase in the concentration of $O(^3P)$ atoms [*Popov*, 2001].

[12] The assumptions of constant pressure and constant neutral density indeed correspond to two heating regimes of the discharge according to whether the breakdown time τ_{br} , defined as the time to heat the channel from ambient temperature (~ 300 K) to the temperature at which the thermal ionization becomes important ($T_{br} \simeq 5000$ K), is more or less than the ratio of the streamer radius r_s to the sound velocity c_s . When $\tau_{br} \leq r_s/c_s$, the role of the channel expansion is small, so that the assumption of constant neutral density employed in 0-D models [e.g., *Naidis*, 1999] and 1-D models [e.g., *Popov*, 2001] is fully justified. At $\tau_{br} > r_s/c_s$, the effects related to the reduction of neutral gas density due to channel expansion become important [*Naidis*, 1999]. At ground pressure, it corresponds to breakdown times $\geq 1 \mu s$ [e.g., *Naidis*, 1999], i.e., similar to the gas dynamics timescales on the order of 0.1–1 μs quoted by *Aleksandrov et al.* [2001], and long enough for equalization of the pressure on timescales of $\sim 1 \mu s$ as discussed by *Popov* [2003]. This last regime can be regarded as occurring under isobaric conditions [*Naidis*, 2005].

[13] Further investigation of the conditions for the appearance of these regimes is made possible by introducing full one-dimensional gas dynamics, i.e., suppressing the hypotheses of either constant pressure or density in the channel. In comparison with the work by *Popov* [2001], *Popov* [2003] introduces an advection term in the time- and space-dependent equation of electron balance, and uses it to further study the role of each of the two heating regimes described by *Naidis* [1999] in the initiation and development of a leader channel in air. It is shown that, during the initial stage of the channel formation, kinetics effects largely govern the parameters of the heating process. In contrast the rapid increase in the electron density near the axis leads to a decrease in the gas density. As a result, the discharge contracts toward the channel axis and evolves into a highly conducting thin column [*Popov*, 2003].

[14] *Naidis* [2005] extends the 1-D steady state models previously developed by *Benilov and Naidis* [2003, 2005] for investigation of low-current discharges in atmospheric pressure air, and discharges in a flow of preheated air. *Naidis*

[2005] tests the conditions of existence of the heating regimes under the assumption of constant pressure or constant neutral gas density. This model is employed in the framework of the study of the dynamics of streamer breakdown of short nonuniform air gap and leads to the conclusion that streamer-to-spark transition at values of $E/N \gtrsim 80$ Td (1 Td = 10^{-17} V \cdot cm 2) may be described with sufficient accuracy under the approximation of constant gas density; at $E/N \lesssim 70$ Td, the transition may be described under the approximation of constant pressure [*Naidis*, 2005]. The obtained model breakdown times are compared with experimental results obtained by *Černák et al.* [1995] and *Larsson* [1998].

[15] Using a model similar to that introduced by *Popov* [2003], *Popov* [2009] recently suggested that the formation of a leader channel in air, and consequently the heating of streamer discharges occurs in two stages: one based on the kinetics processes occurring at an essentially constant gas density on timescales much shorter than the characteristic gas dynamic time, and another in which gas dynamic rarefaction of the channel becomes dominant. In other words, this work suggests that the two regimes described by *Naidis* [2005] would occur successively rather than simultaneously.

[16] The model developed in the present paper includes all the components previously incorporated in the model of spark discharges and summarized in the literature review above. Our kinetic approach does not directly adopt the most recent complex kinetics schemes involving several tens of species and several hundreds of reactions [e.g., *Sentman et al.*, 2008a, 2008b; *Gordillo-Vázquez*, 2008; *Flitti and Pancheshnyi*, 2009] but it identifies the dominant reactions relevant to the problem of air heating in the streamer channel and investigates their impact on the streamer-to-spark transition dynamics. There are two principal approaches that are used in the existing literature for modeling studies of air heating effects in streamer discharges. *Marode* [1983] provides an excellent review of related approaches including their relevance to practical systems and the external circuit considerations driving the discharge. The first one usually postulates either a time-dependent or a stationary current and derives time dynamics of the electric field, conductivity and other parameters of the channel assuming continuity of the current along the channel [e.g., *Aleksandrov et al.*, 2001; *Benilov and Naidis*, 2003; *Bazelyan et al.*, 2007; *Popov*, 2001, 2003, 2009]. The second approach assumes a constant value of the electric field in the channel and then self-consistently evaluates dynamics of other discharge parameters (i.e., conductivity, current, gas temperature, etc.) [*Marode et al.*, 1979; *Bastien and Marode*, 1985; *Aleksandrov et al.*, 1998; *Naidis*, 1999, 2005]. As is demonstrated in the above cited literature, the second approach describes very well a situation after the streamer bridges a relatively short gap with a constant applied voltage, and there are several related experiments conducted under controlled laboratory conditions at ground and near-ground air pressures in which streamer-to-spark transition times have been accurately measured [e.g., *Černák et al.*, 1995; *Larsson*, 1998]. The present study reports results relevant to the second approach. The related model set up is motivated by the possibility to carefully test the model-calculated transition times in comparison with experimental data. The goal of the present investigation is to conduct a systematic study of the gas

Table 1. Parameters for the Model of Streamer-to-Spark Transition

Parameter	Symbol	Value at Sea Level	Scaling Property
Domain size	L_r	2 mm	$\propto(N/N_0)^{-1}$
Streamer radius	r_s	0.2 mm	$\propto(N/N_0)^{-1}$
Space step	δr	4 μm	$\propto(N/N_0)^{-1}$
Time step	δt	$0.1 \times \min(\delta r/c_s, \tau_{VT_{N_2, O_2}}, \tau_{VT_0})$	$\propto(N/N_0)^{-1}$
Electron mobility ^a	μ_e	$\sim 5 \times 10^{-2} \text{ V} \cdot \text{m}^2 \text{ s}^{-1}$	$\propto(N/N_0)^{-1}$
Positive ion mobility	μ_+	$2.5 \times 10^{-4} \text{ V} \cdot \text{m}^2 \text{ s}^{-1}$	$\propto(N/N_0)^{-1}$
Negative ion mobility	μ_-	$2.2 \times 10^{-4} \text{ V} \cdot \text{m}^2 \text{ s}^{-1}$	$\propto(N/N_0)^{-1}$
Initial gas temperature	T_g	300 K	$\propto(N/N_0)^0$
Initial vibrational temperature of N_2	T_v	300 K	$\propto(N/N_0)^0$
Final gas temperature	T_{br}	5000 K	$\propto(N/N_0)^0$
Fraction of N_2 in air	x_{N_2}	0.79	$\propto(N/N_0)^0$
Fraction of O_2 in air	x_{O_2}	0.21	$\propto(N/N_0)^0$
Average mass of air particle	m_g	$4.82 \times 10^{-26} \text{ kg}$	$\propto(N/N_0)^0$
Mass of N_2 molecule	m_{N_2}	$4.64 \times 10^{-26} \text{ kg}$	$\propto(N/N_0)^0$
Mass of O_2 molecule	m_{O_2}	$5.31 \times 10^{-26} \text{ kg}$	$\propto(N/N_0)^0$
Quantum of vibrational energy	ΔE_v	0.29 eV	$\propto(N/N_0)^0$
Applied electric field	E	14–24 kV/cm	$\propto(N/N_0)^1$
Initial gas density	N	$2.5 \times 10^{19} \text{ cm}^{-3}$	$\propto(N/N_0)^1$
Initial pressure	p	10^5 Pa	$\propto(N/N_0)^1$
Initial O_2^- density	$n_{O_2^-}$	$2 \times 10^{14} \text{ cm}^{-3}$	$\propto(N/N_0)^2$
Initial electron density	n_e	$2 \times 10^{14} \text{ cm}^{-3}$	$\propto(N/N_0)^2$

^aThe electron mobility depends on the reduced electric field E/N [e.g., *Morrow and Lowke, 1997*].

dynamics and chemical kinetics of the streamer-to-spark transition at different air densities. The set up of our model is similar to that reported by *Naidis* [2005]. We extend this previous work by studying scaling properties of air heating for a broad range of air densities corresponding to altitudes of 0–70 km in the Earth atmosphere.

2. Model Formulation

[17] The model, which we developed for the studies of the effective time τ_{br} of the initial stage of air heating in the channel of positive streamers up to temperature $T_{br} = 5000 \text{ K}$, is one-dimensional axisymmetric and axially invariant (i.e., only dependent on the time t and the radial coordinate r in the cylindrical coordinate system). The model couples a zero-dimensional kinetics scheme with a fully one-dimensional gas dynamics model. It allows the investigation of streamer-to-spark transition at various air densities, or equivalently at various altitudes in the Earth atmosphere. At ground pressure (10^5 Pa), the discharge is modeled in a short air gap of size $d = 1 \text{ cm}$ with the constant applied voltage U . During most of the heating time, after the streamer bridged the gap, the applied electric field E in the gap can be assumed to be uniform along the axis [e.g., *Naidis, 1999, 2005*] and is given by $E = (U - U_c)/d$, where U_c is the voltage drop at the cathode ($U_c = 0.2 \text{ kV}$). The channel has a constant radius r_s taken to be equal to 0.2 mm. In addition, the radial distribution of the electronic conductivity σ_e and ionic conductivity σ_i are assumed to be Gaussian: $\sigma_{e,i} = \sigma_{e,i}^0 e^{-r^2/r_s^2}$, where $\sigma_{e,i}^0$ are the values of the electronic and ionic conductivities on the axis of the channel at $r = 0$ [e.g., *Naidis, 1999, 2005*]. This approximation was introduced by *Naidis* [2005] on the basis of 2-D streamer models. It differs from that of *Popov* [2001, 2003], who assumed that the radial dependence of the electron density (and hence of the conductivity) was governed by the advection with the ambient air velocity and by the ambipolar diffusion processes. Recent work by *Akishev et al.* [2007] and *Naidis* [2009] demonstrate substantial variations of the discharge radius during the streamer-to-spark transition. The

Gaussian distributions adopted in the present study, therefore, should be viewed as a model approximation that may need to be refined as part of subsequent development of the model. To model self-similar discharges, such as those in the experimental work by *Tardiveau et al.* [2001], it is necessary to scale the parameters of the model with the neutral density. This scaling is done based on the similarity relations summarized by *Pasko* [2006]. The scaling of the different parameters of the model and their scaling properties are given in Table 1.

[18] The gas dynamics in the model is governed by the Euler equations [e.g., *Marode, 1983, p. 142; Brown, 1991, p. 267; Popov, 2003, 2009*] and includes the equations of conservation of mass, momentum, and energy and the equation of balance of the vibrational energy of N_2 (equations (3)–(6))

$$\frac{\partial \rho}{\partial t} + \nabla \cdot (\rho \vec{v}) = 0, \quad (3)$$

$$\frac{\partial}{\partial t} (\rho \vec{v}) + \nabla \cdot (\rho \vec{v} \vec{v}) = -\nabla p, \quad (4)$$

$$\frac{\partial \varepsilon}{\partial t} + \nabla \cdot \{(\varepsilon + p) \vec{v}\} = \eta_T Q_e + Q_i + Q_{VT}, \quad (5)$$

$$\frac{\partial \varepsilon_v}{\partial t} + \nabla \cdot (\varepsilon_v \vec{v}) = \eta_V Q_e - Q_{VT}, \quad (6)$$

where ρ , \vec{v} , p , ε , and ε_v represent the mass density, velocity, pressure, energy density, and vibrational energy density of N_2 in the channel, respectively. The total Joule energy deposition rate per unit volume Q is divided into its electronic component $Q_e = \sigma_e E^2$ and ionic component $Q_i = \sigma_i E^2$, such that $Q = Q_e + Q_i$. The Q_{VT} term in equations (5) and (6) describes the transfer of energy from the vibrational energy levels of nitrogen to the translational energy of the gas. The energy density ε is defined as $\varepsilon = \rho (\vec{v} \cdot \vec{v})/2 + p/(\gamma - 1)$, where γ is the

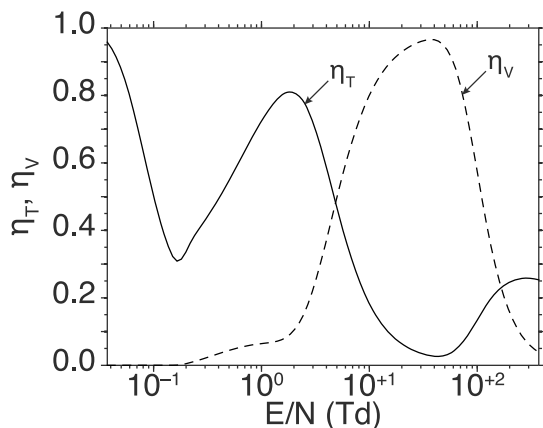


Figure 2. Fractions of Joule energy spent in fast heating η_T (solid line) and vibrational excitation of N_2 molecules η_V (dashed line) as a function of the applied reduced field E/N in Td. The results are based on BOLSIG+ software calculations [Hagelaar and Pitchford, 2005]. The MATLAB function used in the plotting of Figure 2 is freely available to the readers at <http://pasko.ee.psu.edu/air>.

specific heat ratio, assumed to be constant and equal to 1.4. In fact, the specific heat ratio depends on the gas composition and varies with temperature, in particular, for $T_g \gtrsim 2000$ K. But for all the results presented in this work, $T_g \gtrsim 2000$ K means that the system already enters the phase of exponential increases of the gas temperature and is close to the spark stage (see discussion in section 3 and Figures 6a and 8a). Thus, the change of the specific heat ratio has a small influence on our results. The quantities η_T and η_V are the fractions of the Joule energy transferred directly to gas heating (“fast heating”) and to the vibrational energy levels of the nitrogen molecules, respectively. In our calculations of η_T and η_V , we assume an air mixture consisting of 78.11% of nitrogen, 20.91% oxygen, and 0.98% argon. The rates of energy losses by electrons per unit volume (in $\text{eV m}^{-3} \text{s}^{-1}$) in the various collisional processes (see below) are obtained from the BOLSIG+ software [Hagelaar and Pitchford, 2005]. They include the energy losses in elastic collisions, excitation of rotational, vibrational and electronic levels, and ionization of N_2 molecules, denoted by $q_{\text{ela}}^{N_2}$, $q_{\text{rot}}^{N_2}$, $q_{\text{vib}}^{N_2}$, $q_{\text{elec}}^{N_2}$, and $q_{\text{ion}}^{N_2}$, respectively; elastic collisions, excitation of rotational, vibrational and electronic levels, and ionization of O_2 molecules, denoted by $q_{\text{ela}}^{O_2}$, $q_{\text{rot}}^{O_2}$, $q_{\text{vib}}^{O_2}$, $q_{\text{elec}}^{O_2}$, and $q_{\text{ion}}^{O_2}$, respectively; and elastic collisions, excitation of electronic levels, and ionization of Ar atoms, denoted by $q_{\text{ela}}^{\text{Ar}}$, $q_{\text{elec}}^{\text{Ar}}$, and $q_{\text{ion}}^{\text{Ar}}$, respectively. Having introduced the fractions η_{β}^{α} for energy losses for a given species α in the process β as $\eta_{\beta}^{\alpha} = q_{\beta}^{\alpha} / \sum_{\alpha, \beta} q_{\beta}^{\alpha}$, the quantities η_T and η_V are given by the following equations [e.g., Popov, 2001]:

$$\eta_T = (\eta_{\text{ela}}^{N_2} + \eta_{\text{ela}}^{O_2} + \eta_{\text{ela}}^{\text{Ar}}) + (\eta_{\text{rot}}^{N_2} + \eta_{\text{rot}}^{O_2}) + \eta_{\text{vib}}^{O_2} + 0.3 \times (\eta_{\text{elec}}^{N_2} + \eta_{\text{elec}}^{O_2} + \eta_{\text{elec}}^{\text{Ar}}) \quad (7)$$

$$\eta_V = \eta_{\text{vib}}^{N_2} \quad (8)$$

In our calculations of η_T represented by (7), we assumed that 30% of the energy expended on the excitation of the electronic degrees of freedom of the molecules is directly transferred to gas heating [Aleksandrov et al., 1998; Naidis, 1999; Popov, 2001]. Figure 2 shows the values of η_T and η_V for the range of reduced electric field E/N from 3.72×10^{-2} Td to 3.72×10^2 Td calculated from (7) and (8). We note that in our model E is assumed to be uniform and constant and N varies with r and t . These variations are reflected in the changes in η_T and η_V entering in equations (5) and (6).

[19] The electronic conductivity at $r = 0$ is defined as: $\sigma_e^0 = q_e \mu_e n_e$, where q_e , μ_e , and n_e are the electronic charge, mobility, and number density of electrons obtained using the kinetics scheme. Similarly, the ionic conductivity at $r = 0$ is defined as: $\sigma_i^0 = \sum_{\alpha} q_{\alpha} \mu_{\alpha} n_{\alpha}$, where α represents the following ions: O_2^+ , O_4^+ , $O_2^+ N_2$, O^- , O_2^- , and O_3^- , and where q_{α} , μ_{α} and n_{α} are the charge, mobility, and number density of the species α also obtained using the kinetics scheme (see discussion below in this section). The positive and negative ions mobilities are given by $\mu_+ = 2.5 \times 10^{-4} \text{ V} \cdot \text{m}^2 \text{ s}^{-1}$ and $\mu_- = 2.2 \times 10^{-4} \text{ V} \cdot \text{m}^2 \text{ s}^{-1}$ at ground pressure and scale inversely proportionally with the gas density ($\propto N_0/N$) [Zhao et al., 1995]. The electronic mobility μ_e is calculated as a function of the reduced electric field E/N using the approach specified by Morrow and Lowke [1997]. Similarly to the approach used by Naidis [2005] the radial dependence of the electronic and ionic Joule energy deposition rates (Q_e and Q_i , respectively) is assumed to be Gaussian along the r axis, and the related terms are expressed as $Q_e = \sigma_e^0 E^2 e^{-r^2/r_e^2}$ and $Q_i = \sigma_i^0 E^2 e^{-r^2/r_i^2}$, respectively.

[20] The transfer of energy from the vibrational energy levels of molecular nitrogen to translational energy Q_{VT} is expressed as $Q_{VT} = [\varepsilon_v - \varepsilon_{v, \text{eq}}(T_g)] / \tau_{VT}$, where $1/\tau_{VT} = 1/\tau_{VT, N_2, O_2} + 1/\tau_{VT, O}$. The quantities T_g , T_v , ε_v , and $\varepsilon_{v, \text{eq}}(T_g)$ are the gas temperature, the vibrational temperature of N_2 molecules, vibrational energy per unit volume of nitrogen molecules at T_v , and the equilibrium value of ε_v at the temperature $T_v = T_g$, respectively [e.g., Naidis, 1999; Popov, 2003]. The timescales τ_{VT, N_2, O_2} and $\tau_{VT, O}$ are the timescales describing the relaxation of the vibrational energy of the vibrationally excited N_2 molecules into the translational energy of air molecules. We note that our model formulation explicitly includes a term containing $\tau_{VT, O}$, which describes the efficient quenching of vibrational excitation of N_2 by atomic oxygen [Aleksandrov et al., 1997, and references therein]. From, e.g., Naidis [2007] we have: $\varepsilon_v = n_{N_2} \frac{\Delta E_v}{e^{\Delta E_v / k_B T_v - 1}}$, where ΔE_v is the quantum of vibrational energy of N_2 molecules ($\Delta E_v = 0.29$ eV), and k_B is the Boltzmann constant. The timescale τ_{VT, N_2, O_2} is related to the gas temperature and pressure as $\tau_{VT, N_2, O_2} = 6.5 \times 10^{-4} e^{137/T_g[\text{K}]^{1/3}} / p[\text{Pa}]$ s [e.g., Mnatsakanyan and Naidis, 1985], and $\tau_{VT, O}$ depends on both the gas temperature T_g and the number density of atomic oxygen n_O as: $\tau_{VT, O} = 1/(n_O[\text{cm}^{-3}] 1.07 \times 10^{-10} e^{-69.9/T_g[\text{K}]^{1/3}})$ s [e.g., Taylor, 1974]. We note that T_v , T_g , and τ_{VT, N_2, O_2} radial dependencies can be calculated from ρ , \vec{v} , ε , and ε_v . We use the on-axis value of n_O provided by the 0-D kinetics scheme (see below) to estimate the value of $\tau_{VT, O}$. The results of the present work are not sensitive to this approximation.

[21] The system of equations (3)–(6) is discretized using a finite-difference method [e.g., Potter, 1973, pp. 15–17] and solved using a second-order Lax-Wendroff scheme [e.g., Press et al., 1992, p. 844]. The time step δt is related to

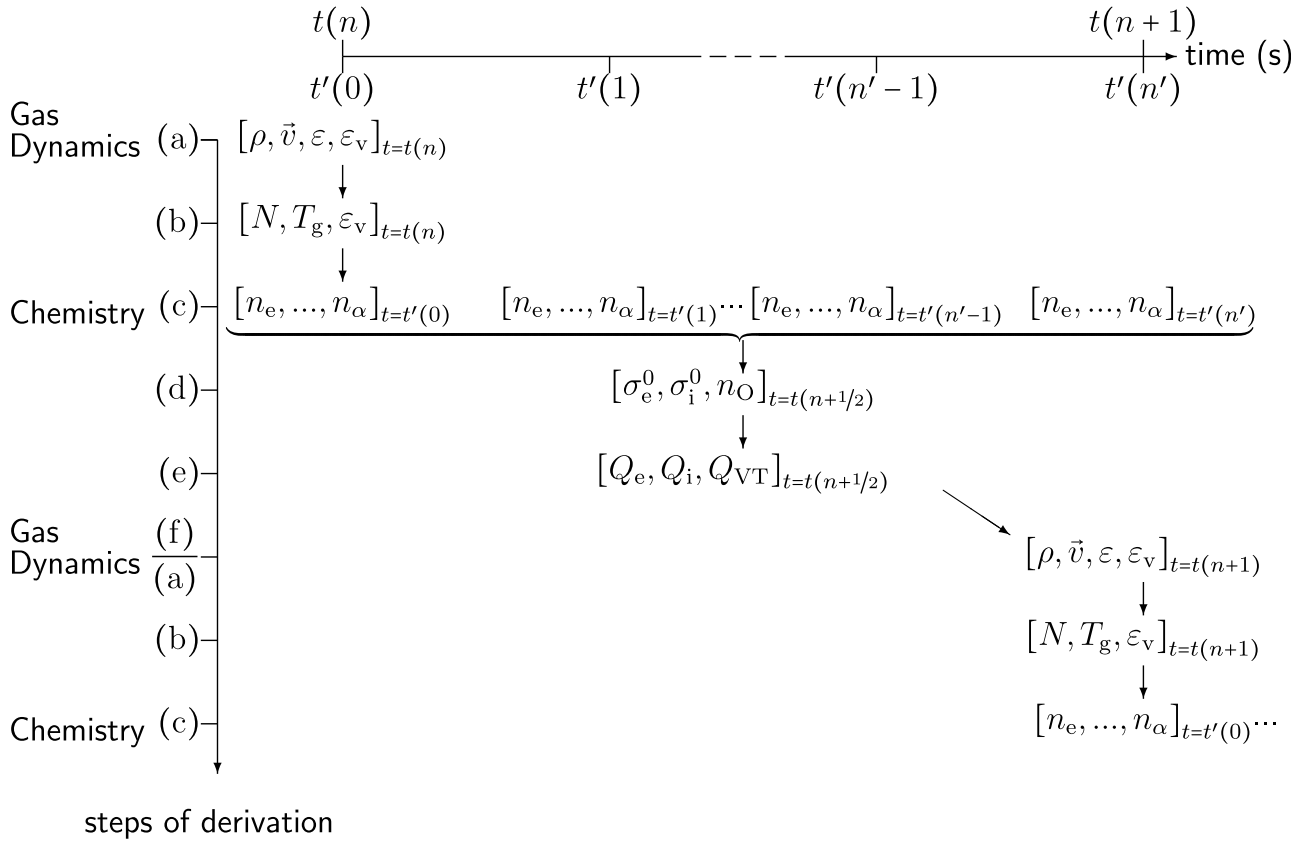


Figure 3. Algorithm for the 1-D axisymmetric, axially invariant model of streamer-to-spark transition. The time notation t represents the time line for the gas dynamics model and t' denotes that of the kinetics scheme. If ρ , \vec{v} , ε , and ε_v are known at $t(n)$ (step a), then the model calculates the values of N , T_g , and ε_v at step b and uses them as input values for the kinetics scheme to derive the densities of each species α in the interval $[t'(0), t'(n')]$ (step c). Then the model calculates the electronic and ionic conductivities of the plasma σ_e^0 and σ_i^0 and density of atomic oxygen on the axis ($r = 0$) at $t(n + 1/2)$ by averaging the values of σ_e^0 , σ_i^0 , and n_O calculated at $t = t'(0)$ and $t = t'(n')$ (step d). Afterward, the terms corresponding to the electronic and ionic Joule energy deposition per unit volume Q_e and Q_i and energy transfer from the vibrational energy levels of nitrogen to translational energy Q_{VT} per unit volume are calculated at every point r of the simulation domain at $t = t(n + 1/2)$ (step e). Finally the values of ρ , \vec{v} , ε , and ε_v are calculated at $t(n + 1)$ using the quantities obtained from steps a and e (step f/a). The process is repeated until T_g reaches a breakdown value $T_{br} = 5000$ K.

the space step δr and to the timescales of the vibrational-translational relaxation through the relationship: $\delta t < \min(\delta r/c_s, \tau_{VT_{N_2, O_2}}, \tau_{VT_O})$, where c_s is the sound velocity in the gas: $c_s = \sqrt{\gamma p/\rho}$. This condition satisfies the Courant-Friedrichs-Lewy stability criterion [e.g., Courant et al., 1928; Potter, 1973, p. 63]. At the beginning of each time step, the gas dynamics model takes for input the values of ρ , \vec{v} , ε , and ε_v at the end of the previous step to calculate the quantities η_T , η_V , Q_{VT} , and p . The terms Q_e , Q_i , and Q_{VT} are obtained from the electron, ion, and atomic oxygen densities calculated by the 0-D kinetics scheme described hereafter. Note that we use the notation $Q = (\sigma_e^0 + \sigma_i^0)E^2 e^{-r^2/r_s^2}$ to represent the Joule heating term consisting of electron and ion components.

[22] The kinetics scheme developed for the studies presented in this work involves 17 species (electrons e; neutral particles N_2 , O_2 , O, N, NO, $O_2(a^1\Delta_g)$, $N_2(A^3\Sigma_u^+)$, $N_2(B^3\Pi_g)$, $N_2(C^3\Pi_u)$, $N_2(a^1\Sigma_u)$; negative ions O^- , O_2^- , O_3^- ; and positive

ions O_2^+ , O_4^+ , $O_2^+N_2$) with 67 reactions summarized in Table 2. The model rates are taken from Vallance-Jones [1974], Kosygi et al. [1992], Lowke [1992], Walter et al. [1994], Aleksandrov et al. [1995], Morrow and Lowke [1997], Popov [2001], Benilov and Naidis [2003], and Liu and Pasko [2004]. The model accounts for the effects of gains in electron energy in collisions with vibrationally excited N_2 on the rate constants of processes involving electron impact collisions (reactions R2, R3 and R28–R30 in Table 2) [Benilov and Naidis, 2003]. The system of kinetic equations is solved to describe the time dynamics of the density of each species α on the axis of the discharge, i.e., using a 0-D approximation [Naidis, 1999, 2005]. In particular, the general balance equation for the electron number density ($\alpha = e$) can be written in the form [Naidis, 1999]

$$\frac{dn_e}{dt} = (F_{ion} + F_{step} + F_d - F_{a_2} - F_{a_3} - F_{rec})n_e, \quad (9)$$

Table 2. List of Reactions^a

Reactions	Rate Constant	Units	References	Comments
R1	$M + e \rightarrow O_2^+ + e + e$	ν_i 1/s	Generation of Electrons by Direct Ionization: F_{ion} Morrow and Lowke [1997, reaction (A1/A2)]	$\nu_i = k_{ion,O_2} [O_2] + k_{ion,N_2} [N_2]$; $M = N_2, O_2$
R2 ^a	$NO + e \rightarrow NO^+ + e + e$	$5.0 \times 10^{-9} \exp(-460/(E/N))F$ cm ³ /s	Morrow and Lowke [1997, reaction (A1/A2)]	
R3 ^a	$O + e \rightarrow O^+ + e + e$	$4.0 \times 10^{-9} \exp(-713/(E/N))F$ cm ³ /s	Benilov and Naidis [2003, reaction (3)]	$O^+ + O_2 \rightarrow O_2^+ + O$
R4	$N_2(A) + N_2(a) \rightarrow N_4^+ + e$	5×10^{-11} cm ³ /s	Benilov and Naidis [2003, reaction (4)]	$N_4^+ + O_2 \rightarrow O_2^+ + N_2 + N_2$
R5	$N_2(a) + N_2(a) \rightarrow N_4^+ + e$	2×10^{-10} cm ³ /s	Kossyi et al. [1992, reaction (25)] Kossyi et al. [1992, reaction (26)]	$N_4^+ + O_2 \rightarrow O_2^+ + N_2 + N_2$
R6	$O_2 + e \rightarrow O^- + O$	ν_{a_2} 1/s	Loss of Electrons by Two- and Three-Body Attachment Processes: $F_{a_2} + F_{a_3}$ Morrow and Lowke [1997, reaction (A3/A4)]	$\nu_{a_2} = k_{a_2} [O_2]$
R7	$O_2 + e + M \rightarrow O_2^- + M$	ν_{a_3} 1/s	Morrow and Lowke [1997, reaction (A5)]	$\nu_{a_3} = k_{a_3} [O_2][M]$; $M = N_2, O_2$
R8	$O_2 + O + e \rightarrow O + O_2^-$	10^{-31} cm ⁶ /s	Kossyi et al. [1992, reaction (48)]	
R9	$O_2^+ + e \rightarrow O + O$	$2 \times 10^{-7} (300/T_e)$ cm ³ /s	Loss of Electrons by Electron-Ion Recombination: F_{rec} Kossyi et al. [1992, reaction (40)]	
R10	$O_2^+ + e + M \rightarrow O_2 + M$	$6 \times 10^{-27} (300/T_e)^{1.5}$ cm ⁶ /s	Kossyi et al. [1992, reaction (44)]	$A = O_2^+$; $M = O_2, N_2$
R11	$O_4^+ + e \rightarrow O_2 + O_2$	$1.4 \times 10^{-6} (300/T_e)^{1/2}$ cm ³ /s	Kossyi et al. [1992, reaction (30)]	
R12	$O_2^+ N_2 + e \rightarrow O_2 + N_2$	$1.3 \times 10^{-6} (300/T_e)^{1/2}$ cm ³ /s	Kossyi et al. [1992, reaction (34)]	
R13	$O_2^- + O_2(a) \rightarrow O_2 + O_2 + e$	2×10^{-10} cm ³ /s	Generation of Electrons by Detachment: F_d Kossyi et al. [1992, reaction (58)]	
R14	$O_2^- + N_2(A) \rightarrow O_2 + N_2 + e$	2.1×10^{-9} cm ³ /s	Kossyi et al. [1992, reaction (60)]	
R15	$O^- + N_2 \rightarrow N_2O + e$	9×10^{-13} cm ³ /s	Benilov and Naidis [2003, reaction (22)]	
R16	$O^- + O \rightarrow O_2 + e$	5×10^{-10} cm ³ /s	Benilov and Naidis [2003, reaction (23)]	
R17	$O_2 + O \rightarrow O_3 + e$	1.5×10^{-10} cm ³ /s	Benilov and Naidis [2003, reaction (25)]	
R18	$O_3^- + O \rightarrow O_2 + O_2 + e$	3×10^{-10} cm ³ /s	Benilov and Naidis [2003, reaction (26)]	
R19	$O^- + O_2(a) \rightarrow O_3 + e$	2.2×10^{-9} cm ³ /s	Kossyi et al. [1992, reaction (62)]	
R20	$O^- + N_2(A) \rightarrow O + N_2 + e$	2.2×10^{-9} cm ³ /s	Kossyi et al. [1992, reaction (64)]	
R21	$O^- + NO \rightarrow NO_2 + e$	2.6×10^{-10} cm ³ /s	Benilov and Naidis [2003, reaction (24)]	
R22	$O_2^- + O_2 \rightarrow O_2 + O_2 + e$	$2 \times 10^{-10} \exp(-0.52/T_{e2}) \frac{1-e^{-\theta}}{1-e^{-\theta/T_{e2}}}$ cm ³ /s	Benilov and Naidis [2003, reaction (21)]	
R23	$O_2 + e \rightarrow O_2(a) + e$	$\nu_{O_2(a)}$ 1/s	Electron Impact Excitation of Metastable State: F_{ex} Aleksandrov et al. [1995, reaction (8)]	$\nu_{O_2(a)} = k_{O_2(a)} [O_2]$
R24	$N_2 + e \rightarrow N_2(A) + e$	$\nu_{N_2(A)}$ 1/s	Aleksandrov et al. [1995, reaction (4)]	$\nu_{m,N_2} = k_{N_2(A)} [N_2]$
R25	$N_2 + e \rightarrow N_2(a) + e$	$\nu_{N_2(a)}$ 1/s	Aleksandrov et al. [1995, reaction (6)]	$\nu_{N_2,a} = k_{N_2(a)} [N_2]$
R26	$N_2 + e \rightarrow N_2(B) + e$	ν_{1P} 1/s	Aleksandrov et al. [1995, reaction (5)]	$\nu_{1P} = k_{1P} [N_2]$
R27	$N_2 + e \rightarrow N_2(C) + e$	ν_{2P} 1/s	Aleksandrov et al. [1995, reaction (7)]	$\nu_{2P} = k_{2P} [N_2]$
R28 ^a	$N_2 + e \rightarrow N + N + e$	$5.0 \times 10^{-9} \exp(-646/(E/N))F$ cm ³ /s	Electron Impact Dissociation: F_{di} Benilov and Naidis [2003, reaction (5)]	
R29 ^a	$O_2 + e \rightarrow O(^2P) + O(^3P) + e$	$F\nu_{O(^2P)}$ 1/s	Aleksandrov et al. [1995, reaction (10)]	Benilov and Naidis [2003, reaction (6)] ^b
R30 ^a	$O_2 + e \rightarrow O(^3P) + O(^1D) + e$	$F\nu_{O(^1D)}$ 1/s	Aleksandrov et al. [1995, reaction (11)]	
R31	$N + NO \rightarrow O + N_2$	$1.1 \times 10^{-10} T_g [\text{eV}]^{1/2}$ cm ³ /s	Ground States Chemistry: F_{gs} Benilov and Naidis [2003, reaction (15)]	
R32	$N + O_2 \rightarrow O + NO$	$1.2 \times 10^{-10} T_g [\text{eV}] \exp(-0.27/T_g [\text{eV}])$ cm ³ /s	Benilov and Naidis [2003, reaction (17)]	

Table 2. (continued)

Reactions	Rate Constant	Units	References	Comments
R33 ^c	$N_2(B) \rightarrow N_2(A) + h\nu$ (1PN ₂)	1.7×10^5	<i>Active States Chemistry and Collisional and Radiative Deactivation: F*</i> <i>Liu and Pasko [2004]</i>	<i>Walter et al. [1994]^b</i>
R34 ^c	$N_2(C) \rightarrow N_2(B) + h\nu$ (2PN ₂)	2.0×10^7	<i>Liu and Pasko [2004]</i>	<i>Walter et al. [1994]^b</i>
R35 ^c	$N_2(B) + N_2 \rightarrow N_2 + N_2$	1.0×10^{-11}	Table 4.7 of <i>Vallance-Jones [1974]</i>	
R36 ^c	$N_2(C) + O_2 \rightarrow N_2 + O_2$	3.0×10^{-10}	Table 4.7 of <i>Vallance-Jones [1974]</i>	
R37	$O_2(a) + O_2 \rightarrow O_2 + O_2$	$2.2 \times 10^{-18} (T_e/300)^{0.8}$	<i>Kossyi et al. [1992, reaction (123)]</i> <i>Kossyi et al. [1992, reaction (102)]</i>	<i>Lowke [1992, reaction (6)]^b</i>
R38	$N_2(A) + O \rightarrow NO + N(D)$	7×10^{-12}	<i>Popov [2001, reaction (4)]</i>	
R39 ^c	$N_2(A) + N_2(A) \rightarrow N_2(B) + N_2$	7.7×10^{-11}	<i>Popov [2001, reaction (3)]</i>	<i>Kossyi et al. [1992, reaction (104)]^b</i>
R40 ^c	$N_2(A) + N_2(A) \rightarrow N_2(C) + N_2$	1.6×10^{-10}	<i>Kossyi et al. [1992, reaction (108)]</i>	<i>Kossyi et al. [1992, reaction (104)]^b</i>
R41	$N_2(A) + O \rightarrow N_2 + O(S)$	2.1×10^{-11}	<i>Kossyi et al. [1992, reaction (100)]</i>	
R42	$N_2(A) + O_2 \rightarrow N_2 + O + O$	2.54×10^{-12}	<i>Kossyi et al. [1992, reaction (115)]</i>	
R43	$N_2(a) + O_2 \rightarrow N_2 + O + O$	2.8×10^{-11}	<i>Kossyi et al. [1992, reaction (115)]</i>	
R44	$A^- + B^+ \rightarrow A + B$	$2 \times 10^{-7} (300/T_e)^{0.5}$	<i>Ion-Ion Recombination: F_{ii}</i> <i>Kossyi et al. [1992, reaction (1)]</i>	$A^- = O^-; B^+ = O_2^+$ $A^- = O_2^-; B^+ = O_2^+$ $A^- = O_3^-; B^+ = O_2^+$
R45	$O^- + O_2^+ \rightarrow O + O_2$			$A^- = O^-; BC^+ = O_2^+$ $A^- = O^-; BC^+ = O_4^+$ $A^- = O^-; BC^+ = O_2^+N_2$
R46	$O_2^- + O_2^+ \rightarrow O_2 + O_2$			$A^- = O_2^-; BC^+ = O_2^+$ $A^- = O_2^-; BC^+ = O_4^+$ $A^- = O_2^-; BC^+ = O_2^+N_2$
R47	$O_3^- + O_2^+ \rightarrow O + O + O$			$A^- = O_3^-; BC^+ = O_2^+$ $A^- = O_3^-; BC^+ = O_4^+$ $A^- = O_3^-; BC^+ = O_2^+N_2$
R48	$O^- + O_3^+ \rightarrow O + O_2 + O_2$			$A^- = O^-; BC^+ = O_2^+$ $A^- = O^-; BC^+ = O_4^+$ $A^- = O^-; BC^+ = O_2^+N_2$
R49	$O^- + O_2^+N_2 \rightarrow O + O_2 + N_2$			$A^- = O^-; BC^+ = O_2^+$ $A^- = O^-; BC^+ = O_4^+$ $A^- = O^-; BC^+ = O_2^+N_2$
R50	$O_2^- + O_2^+ \rightarrow O_2 + O + O$			$A^- = O_2^-; BC^+ = O_2^+$ $A^- = O_2^-; BC^+ = O_4^+$ $A^- = O_2^-; BC^+ = O_2^+N_2$
R51	$O_2^- + O_4^+ \rightarrow O_2 + O_2 + O_2$			$A^- = O_2^-; BC^+ = O_2^+$ $A^- = O_2^-; BC^+ = O_4^+$ $A^- = O_2^-; BC^+ = O_2^+N_2$
R52	$O_2^- + O_2^+N_2 \rightarrow O_2 + O_2 + N_2$			$A^- = O_2^-; BC^+ = O_2^+$ $A^- = O_2^-; BC^+ = O_4^+$ $A^- = O_2^-; BC^+ = O_2^+N_2$
R53	$O_3^- + O_2^+ \rightarrow O_3 + O + O$			$A^- = O_3^-; BC^+ = O_2^+$ $A^- = O_3^-; BC^+ = O_4^+$ $A^- = O_3^-; BC^+ = O_2^+N_2$
R54	$O_3^- + O_4^+ \rightarrow O_3 + O_2 + O_2$			$A^- = O_3^-; BC^+ = O_2^+$ $A^- = O_3^-; BC^+ = O_4^+$ $A^- = O_3^-; BC^+ = O_2^+N_2$
R55	$O_3^- + O_2^+N_2 \rightarrow O_3 + O_2 + N_2$			$A^- = O_3^-; BC^+ = O_2^+$ $A^- = O_3^-; BC^+ = O_4^+$ $A^- = O_3^-; BC^+ = O_2^+N_2$
R56	$O_4^+ + O_2^+(a) \rightarrow O_2^+ + O_2 + O_2$	10^{-10}	<i>Positive Ions Chemistry: F_i</i> <i>Kossyi et al. [1992, reaction (228)]</i>	
R57	$O_4^+ + O \rightarrow O_2^+ + O_3$	3×10^{-10}	<i>Kossyi et al. [1992, reaction (229)]</i>	
R58	$O_2^+ + O_2 + O_2 \rightarrow O_4^+ + O_2$	$2.4 \times 10^{-30} (300/T_e)^{3.2}$	<i>Kossyi et al. [1992, reaction (167)]</i>	
R59	$O_2N_3 + O_2 \rightarrow O_4^+ + N_2$	10^{-9}	<i>Kossyi et al., reaction (232)</i>	
R60	$O_2^+ + N_2 + N_2 \rightarrow O_2^+N_2 + N_2$	$0.9 \times 10^{-30} (300/T_e)^2$	<i>Kossyi et al. [1992, reaction (168)]</i>	
R61	$O_4^+ + N_2 \rightarrow O_2^+N_2 + O_2$	$4.61 \times 10^{-12} (300/T_e)^{2.5} \exp(-2650/T_e)$	<i>Kossyi et al. [1992, reaction (226)]</i>	
R62	$O_2^+N_2 + N_2 \rightarrow O_2^+ + N_2 + N_2$	$1.1 \times 10^{-6} (300/T_e)^{3.3} \exp(-2357/T_e)$	<i>Kossyi et al. [1992, reaction (231)]</i>	
R63	$O_4^+ + O_2 \rightarrow O_2^+ + O_2 + O_2$	$3.3 \times 10^{-6} (300/T_e)^4 \exp(-5030/T_e)$	<i>Kossyi et al. [1992, reaction (227)]</i>	
R64	$O^- + O_2(a) \rightarrow O_2^- + O$	10^{-10}	<i>Negative Ions Chemistry: F_i</i> <i>Kossyi et al. [1992, reaction (242)]</i>	
R65	$O_2^- + O \rightarrow O_2 + O^-$	3.3×10^{-10}	<i>Kossyi et al. [1992, reaction (237)]</i>	
R66	$O_3^- + O \rightarrow O_2 + O_2$	3.2×10^{-10}	<i>Kossyi et al. [1992, reaction (247)]</i>	
R67	$O^- + O_2 + M \rightarrow O_3^- + M$	$2.8 \times 10^{-32} T_{eM}^{-1}$ $T_{eM} = T_e [eV] + 6.9 \times 10^{-6} (E/N)^2 [eV]$	<i>Benilov and Naidis [2003, reaction (27)]</i>	M = N ₂ , O ₂

^aA correction to account for gains in electron energy in collisions with vibrationally excited nitrogen molecules is introduced by means of the factor $F = e^{Cz/(E/N)^2}$ where $C = 6.5 \times 10^3 \text{ Td}^2$ and $z = e^{-\Delta E/k_B T}$. [*Benilov and Naidis, 2003*].

^bAlternative reference for the given reaction. The reaction number in this reference is provided if available.

^cReactions R32, R33, R34, R35, R38 are used to derive the densities of N₂(B) and N₂(C) in a steady state approximation.

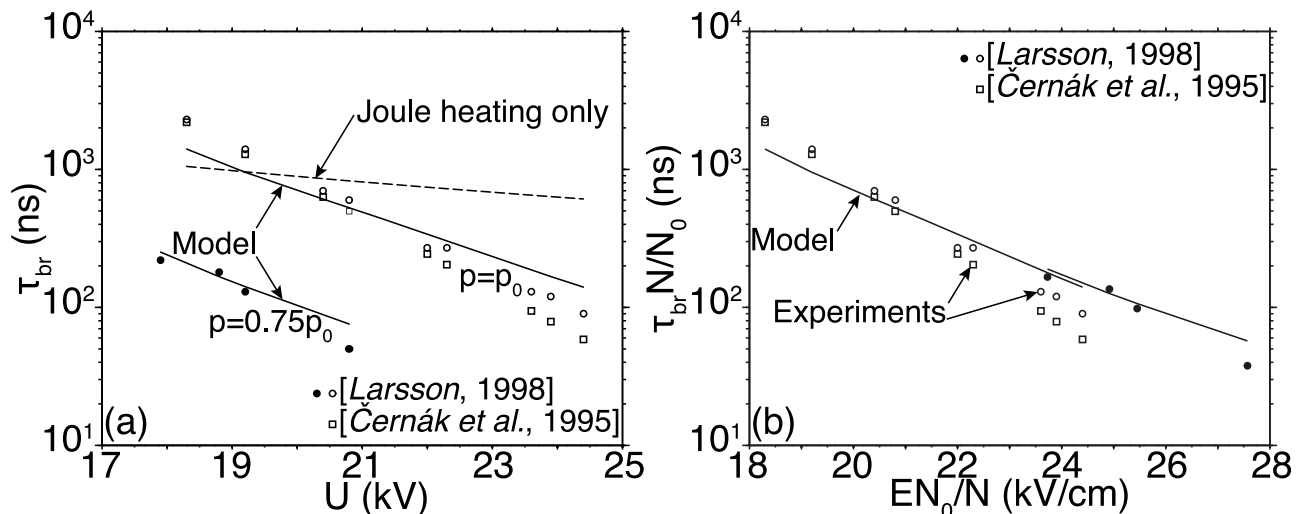


Figure 4. (a) Experimental and modeled streamer-to-spark transition times for various applied voltages. The solid lines represent the transition times under normal pressure ($p = 10^5$ Pa) and reduced pressure ($p = 0.75 \times 10^5$ Pa). The dashed line shows the breakdown time of a Joule heated channel with constant neutral gas density corresponding to $p = 10^5$ Pa and assuming a constant plasma conductivity in the channel. The squares show experimental results obtained by Černák et al. [1995] and the open and solid circles show the results obtained by Larsson [1998]. The data obtained for reduced air pressure are shown with solid circles, and the data taken at ground pressure p_0 are shown with open circles. (b) Same model and experimental data as in Figure 4a but using reduced values of the applied field (EN_0/N) and of the transition times ($\tau_{br}N/N_0$).

where F_{ion} is the rate of direct ionization of N_2 and O_2 ; F_{step} is the sum of the rates of ionization of radicals by the electron impact and associative ionization in collisions of excited N_2 ; F_d , $F_{a,2}$, $F_{a,3}$, and F_{rec} are the rates of detachment, two-body attachment, three-body attachment, and electron-ion recombination, respectively. The source terms corresponding to associative ionization and detachment are not proportional to the electron number density n_e , but the representation of the corresponding terms in the form of (9) is very convenient for purposes of comparison of different processes [Naidis, 1999].

[23] In summary, the model employs a fully 1-D axisymmetric, axially invariant gas dynamics model coupled to a 0-D kinetics scheme according to the algorithm schematically represented in Figure 3. The time integration is ended when the gas temperature T_g reaches the predefined breakdown temperature $T_{br} = 5000$ K. The laboratory data on timescales of air heating in streamer channels at ground and near-ground pressures [Larsson, 1998], and related modeling studies [Naidis, 1999, 2005] indicate that the experimentally measured and previously calculated τ_{br} values are in good agreement with our model results for the range $18 < EN_0/N < 24$ kV/cm (see the results presented in section 3). We emphasize that the combined action of uncertainties in the initial streamer electron density ($n_{e|t=0} = 1-3 \times 10^{14} \text{ cm}^{-3}$), the initial densities of active species in the streamer after the passage of the high electric field pulse associated with the streamer head, and the cathode voltage drop (U_c) lead to estimated combined uncertainty of a factor of two for the model breakdown times τ_{br} reported in section 3. In this work, we choose the same initial conditions as those used by Naidis [2005] ($n_{e|t=0} = 2 \times 10^{14} \text{ cm}^{-3}$, $U_c = 0.2$ kV, and zero initial densities of active species) to demonstrate performance of our model in comparison with results given by Naidis [1999, 2005]. The conclusions derived in the present

work on air-density-dependent scaling of the discharge properties are not sensitive to these assumptions.

3. Results

[24] In this section, we present results of simulations of the streamer-to-spark transition at various altitudes, or equivalently air densities. The results are obtained assuming that the discharge occurs in a domain with radius $L_r = 2$ mm at ground pressure. Based on their experimental results, Tardiveau et al. [2001] suggested that in studies of similarity laws, the entire system should be scaled, and consequently L_r is scaled with neutral density ($L_r \propto 1/N$, see Table 1). The breakdown time τ_{br} is always much less than the ratio $L_r/c_s \simeq 10 \mu\text{s}$ at ground pressure, so that the boundary effects are negligible in the results presented in this work. The scaling of L_r with altitude ensures that this result holds at any altitude.

[25] The 1-D axisymmetric, axially invariant simulation domain of radius L_r is then discretized using 500 space steps of length δr , and consequently δr scales inversely with the neutral density, too ($\delta r \propto 1/N$). The time step δt used in the Lax-Wendroff algorithm in the gas dynamics model (see Figure 3) is chosen as: $\delta t = 0.1 \times \min(\delta r/c_s, \tau_{VT_{N_2, O_2}}, \tau_{VT_O})$ and, therefore, satisfies the Courant-Friedrichs-Lewy condition for stability of the finite-difference numerical scheme as already discussed in section 2. The initial conditions and the other parameters of the model are summarized in Table 1 with their respective scaling properties.

[26] Figure 4a displays the breakdown times τ_{br} at normal and reduced pressure as a function of the applied voltage U . Results are compared with experimental data obtained by Černák et al. [1995] and Larsson [1998]. The solid lines represent the model breakdown times under normal pressure ($p = 10^5$ Pa) and reduced pressure ($p = 0.75 \times 10^5$ Pa). The

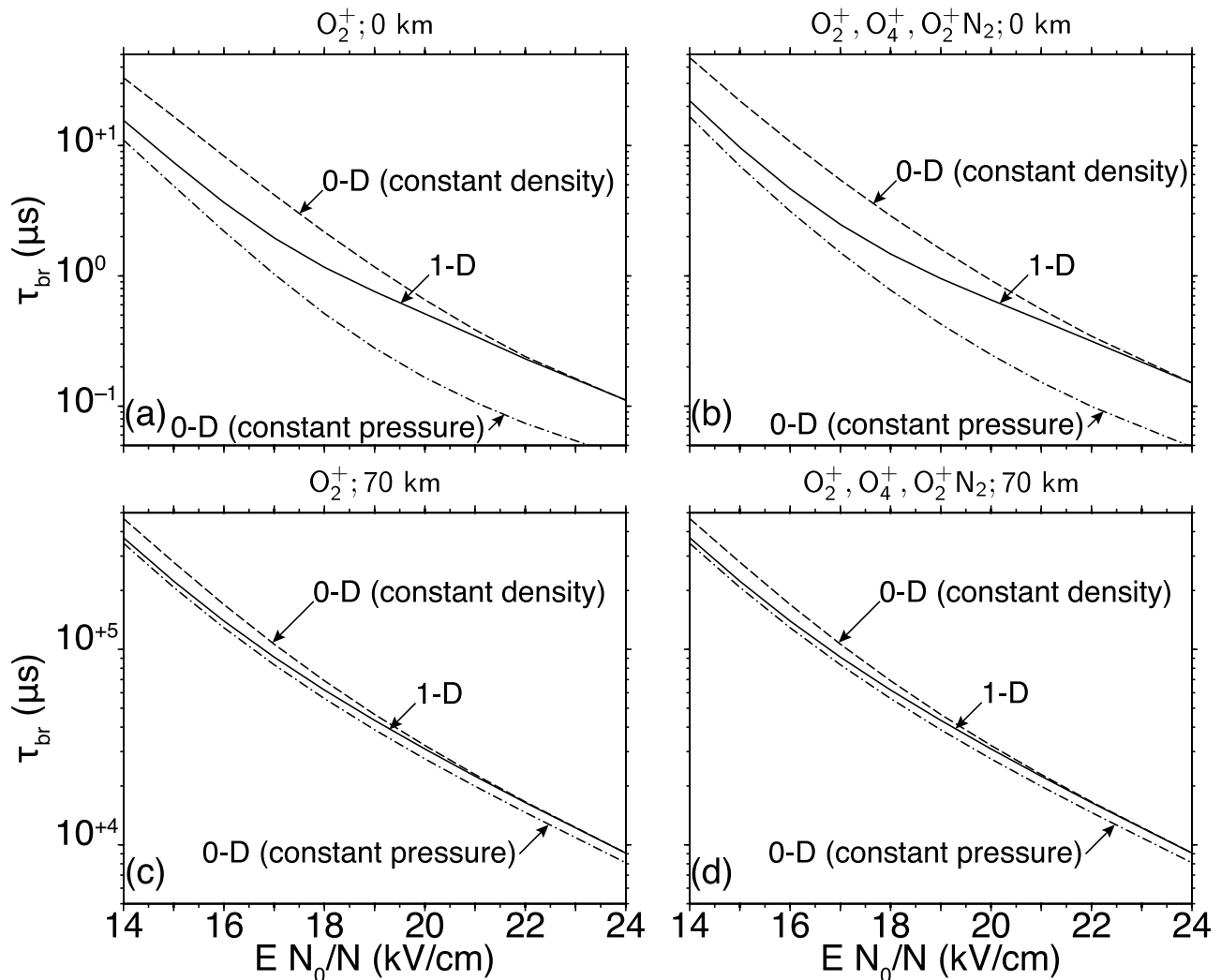


Figure 5. Comparison of 0-D model and 1-D model of section 2 under constant pressure p , constant density N conditions at different altitudes, and for two different kinetic schemes including O_2^+ only at (a) $z = 0$ and (c) $z = 70$ km and O_2^+ , O_4^+ , and $O_2^+N_2$ at (b) $z = 0$ and (d) $z = 70$ km.

dashed line shows the breakdown time in a constant neutral gas density channel assuming a constant conductivity of the channel and that all the power from the system Q is directly used for heating of the plasma. The squares show experimental results reported by Černák *et al.* [1995], and open and solid circles show the results obtained by Larsson [1998]. The data obtained by Larsson [1998] are obtained for a 1 cm long air gap under a constant voltage and are particularly interesting because they represent the experimental setup closest to the model formulated in section 2. Figure 4 shows very good agreement between the model results and the experimental data. In comparison, the estimates based on pure Joule heating (dashed line) demonstrate a completely different slope of variation of τ_{br} as a function of the applied voltage and no good quantitative agreement with the observations. Figure 4b presents the same results but scaled with the neutral density. Both experimental and model transition times are scaled with N as $\tau_{br}N/N_0$ (which is a good estimate of the scaling factor as is shown below in Figure 12), and the applied electric field is represented in its usual reduced form as EN_0/N . We note that the model curves and the data points

obtained at two different pressures both form a monotonic continuous set when represented in the $\tau_{br}N/N_0$ versus EN_0/N format. These results indicate that experimentally measured and modeled transition times agree, and both scale approximately as $\propto 1/N$.

[27] Figure 5 compares the streamer-to-spark transition times obtained using a 0-D model under the assumption of constant density N (dashed lines), a 0-D model under the assumption of a constant pressure p (dot-dashed lines), and the 1-D model described in section 2 (solid lines). The model results are obtained at different altitudes (0 km in Figures 5a and 5b) and 70 km (in Figures 5c and 5d) for two kinetic schemes including electrons, neutral species N_2 , O_2 , O , N , NO , negative ions O^- , O_2^- , O_3^- , and excited species $O_2(a^1\Delta_g)$, $N_2(A^3\Sigma_u^+)$, $N_2(B^3\Pi_g)$, $N_2(C^3\Pi_u)$, $N_2(a^1\Sigma_u)$. The two kinetic schemes differ only through the treatment of positive ions. Only O_2^+ ions are included in the cases of Figures 5a and 5c. The related chemical kinetics can be considered as similar to that presented by Naidis [1999] where O_2^+ was observed as the dominant positive ion. The cases of Figures 5b and 5d include a more complete set of ions: O_2^+ , O_4^+ , and $O_2^+N_2$.

[28] The N_2^+ ions produced as result of electron impact ionization of the N_2 , and the N_4^+ ions produced in associative ionization reactions R4 and R5 (Table 2) are usually assumed to readily convert into O_2^+ ions due to fast charge exchange reactions [e.g., *Aleksandrov and Bazelyan, 1999; Sentman et al., 2008a, 2008b*]. This approximation is fully justified by the timescale of these conversions (~ 1 ns at altitude 0 km), which is much shorter than the timescale of the streamer-to-spark transition. Therefore, we assume in our model that the electron impact ionization of N_2 and the associative ionization reactions directly lead to the production of O_2^+ ions. Similarly, we assume that atomic oxygen ions O^+ produced in reaction R3 (Table 2) very quickly convert to O_2^+ ions via a charge exchange reaction $O^+ + O_2 \rightarrow O_2^+ + O$ that has timescale ~ 30 ns at 0 km and ~ 0.4 ms at 70 km [*Sentman et al., 2008a, 2008b*].

[29] The O_2^+ ions quickly convert into O_4^+ ions through the reaction R58 (Table 2) and into $O_2^+N_2$ ions through the reaction R60 (Table 2). The rate of conversion of $O_2^+N_2$ ions into O_4^+ via the three-body reaction R59 is also very high leading to the predominance of this ion at high air densities (low altitudes). Figures 7 and 9 presented below illustrate that the O_4^+ ion dominates at altitude 0 km, but O_2^+ dominates at 70 km. The positive ion chemistry and the influence of the ion temperature on the results is discussed in sections 4.5 and 4.6. The importance of O_4^+ ions at high air pressures is underscored by the fact that these ions have a very high recombination rate with electrons (R11, Table 2) leading to a slower streamer-to-spark transition. This is confirmed by the direct comparison of the results presented in Figure 5a, which are obtained assuming O_2^+ ions only, and those presented in Figure 5b based on a complete positive ion chemistry including O_2^+ , O_4^+ , and $O_2^+N_2$ ions. We note that although electron impact ionization of NO (R2) is explicitly included in our model, under the studied conditions NO^+ ions do not make any significant contribution to streamer-to-spark transition dynamics.

[30] Figure 5 shows that at any altitude and for both schemes, the 1-D model converges toward the 0-D model under constant density at high-applied electric fields and toward the 0-D model under constant pressure at lower-applied electric field. A significant difference appears from the comparison of the situations described in Figure 5: although at low pressures (Figures 5c and 5d) the differences between constant density and constant pressure streamer-to-spark transition times do not exceed $\sim 25\%$, the results produced by the different models can differ by as much as a factor 2 to 3 at ground pressure. In section 4, we discuss the reasons for those differences. We further emphasize that the results shown in Figure 5b for full chemistry and 1-D geometry overlap those presented at ground pressure in Figure 4a (solid line), when the applied voltage U is converted to the applied reduced electric field EN_0/N in the range $U = 18\text{--}24.5$ kV.

[31] Figures 6, 7, and 10a illustrate the temporal dynamics of the streamer-to-spark transition at altitude 0 km (i.e., at ground pressure $p = 10^5$ Pa) assuming $EN_0/N = 19$ kV/cm and full O_2^+ , O_4^+ , and $O_2^+N_2$ ion chemistry kinetics. The time by which the gas temperature reaches 5000 K is $\tau_{br} = 0.95$ μ s in this case. Figures 6a and 6b represent the evolution of the neutral gas density normalized with the ambient gas density N_{amb} and of the gas pressure p normalized with the ambient

pressure p_{amb} at the altitude of the simulation (0 km). The ratio N/N_{amb} remains constant until $t = 0.2$ μ s, then drops quickly just before reaching the spark stage. Conversely, the ratio p/p_{amb} increases slowly until $t = 0.2$ μ s, when it reaches a plateau for ~ 200 ns, and then increases exponentially. Figure 6c shows the time evolution of the gas temperature T_g (solid line) and of the vibrational temperature T_v of N_2 (dashed line) at the axis of the channel. The temperature T_g increases almost linearly by a few tens of Kelvins until $t \sim 0.5$ μ s, when it starts increasing exponentially. A similar observation can be made about T_v . These dynamics are in good quantitative agreement with those reported previously by *Naidis* [1999, 2005]. The current flowing in the channel $I = \pi r_s^2 (\sigma_i^0 + \sigma_e^0) E^2$ is represented in Figure 6d.

[32] Figures 7a and 7b show the evolution of the densities of charged and neutral particles with time. Note that O_4^+ is the dominant species after 10 ns and until the end of the simulation (i.e., $T_g \geq T_{br}$). In Figure 7c, we illustrate the contributions from the fast heating and the vibrational-translational relaxation to the increase of energy density (and, therefore, to the neutral gas temperature). The contribution from the fast heating and ionic Joule heating remains largely dominant over the energy transfer from vibrational-translational relaxation until the time of the transition. Figure 7d shows the electron generation and loss rates during the transition, and emphasizes the relative importance of the detachment and stepwise ionization processes in the growth of electron density during the streamer-to-spark transition. It is believed that the fast release of electrons in detachment collisions is a critically important process for the fast gas heating in streamer channels [e.g., *Aleksandrov et al., 1997; Naidis, 1999; Vidal et al., 2002; Comtois et al., 2003*]. Figure 10a illustrates the contributions of different processes to the total rate of detachment F_d shown in Figure 7d, indicating in particular the dominant role of $O^- + N_2$, $O^- + O$, and $O_3 + O$ interactions (reactions R15, R16, and R18 in Table 2, respectively) in the rapidly growing detachment rate. These results are in good agreement with the conclusions reached by *Naidis* [1999] indicating that the major cause of spark formation is an increase with time in the electron detachment rate due to the accumulation of oxygen atoms and other active species.

[33] Figures 8, 9, and 10b provide the same information as Figures 6, 7, and 10a at $EN_0/N = 19$ kV/cm only for the altitude 70 km (i.e., at pressure $p \simeq 7$ Pa). In this case, $\tau_{br} = 43.3$ ms. Figure 8c reveals that the initial linear increase in T_g is no longer present, instead, T_g remains constant until the very last stage of the streamer-to-spark transition; then at $t \sim 30$ ms, it increases exponentially. Similarly, the neutral gas density remains constant until the time of exponential increase of T_g , at which point it decreases rapidly (Figure 8a). Interestingly, the behavior of the ratio p/p_{amb} in Figure 8b is significantly simpler than at 0 km, as it presents no variations until $t \sim 30$ ms. Although O_4^+ prevails at 0 km in Figure 7a, Figure 9a emphasizes that O_2^+ remains the dominant positive ion throughout the entire duration of the streamer-to-spark transition at 70 km because of the disappearance of three-body interactions leading to more complex ions, as already noted above. Figure 9d emphasizes the disappearance of the three-body attachment and dramatic reduction in the recombination loss rate of electrons at low air pressures. We

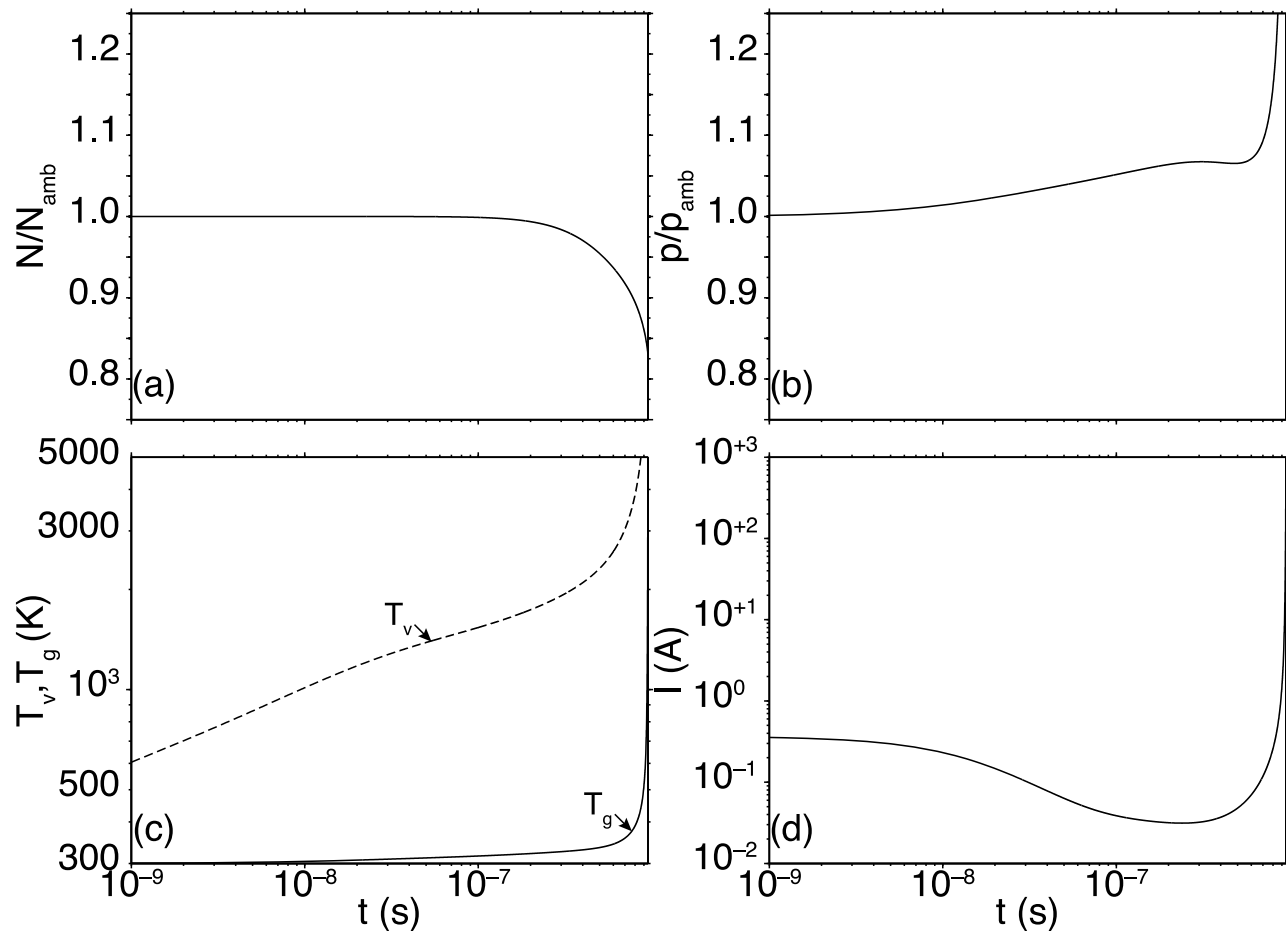


Figure 6. Temporal dynamics of the streamer-to-spark transition at altitude 0 km and $EN_0/N = 19$ kV/cm. (a) Changes in the normalized neutral gas density N/N_{amb} at the axis of the channel, where N_{amb} is the ambient air density at the altitude considered. (b) Variations of the normalized pressure p/p_{amb} at the axis of the channel, where p_{amb} is the ambient pressure at the altitude considered. (c) Evolution of the neutral gas temperature T_g (solid line) and vibrational temperature T_v of N_2 at the axis of the channel (dashed lined). (d) Electric current I flowing along the channel defined as $I = \pi r_s^2 (\sigma_e^0 + \sigma_i^0) E^2$.

emphasize that the reduction of the recombination rate as documented in Figure 9d at low air density in comparison with ground level results shown in Figure 7d is one of the fundamental reasons for acceleration of heating observed at reduced air densities and reported in this paper. The recombination process is described in kinetic equations by terms that contain products of electron and ion densities and, therefore, these terms can be approximately viewed as quadratic with respect to streamer electron density. Because electron density itself scales with air density as $\sim N^2$, the contribution of these quadratic terms quickly becomes negligible in comparison with other processes (i.e., two-body attachment) with reduction of air density N . The two-body attachment process, for example, enters in electron balance equation (9) as $-F_{a_2} n_e$, where $F_{a_2} = \nu_{a_2}$ and ν_{a_2} scales proportionally to N . The recombination term enters in the same equation as $-F_{\text{rec}} n_e$, where F_{rec} is itself proportional to n_e and, therefore, scales as $\propto N^2$, becoming negligible in comparison with two-body processes at low air densities at high altitudes (see Figure 9d). Figure 10b shows that the detachment rate F_d at 70 km is almost exclusively governed by the $\text{O}^- + \text{N}_2$ interaction (reaction R15 in Table 2) until the very last stage

of the transition, when the $\text{O}^- + \text{O}$ interaction (reaction R16 in Table 2) becomes dominant.

[34] Figure 11 shows the distribution of the reduced gas density N/N_{amb} as a function of the radial coordinate at 0 km at $t = 0, 0.3, 0.6,$ and $0.9 \mu\text{s}$ (Figure 11a), and at 70 km at $t = 10, 20, 30$ and 40 ms (Figure 11b). It demonstrates that at higher altitudes the neutral gas density remains almost constant for most of the transition (within $\sim 1\%$ of the initial value until $t \gtrsim 30$ ms), and almost no radial expansion of the channel occurs until the very last stage of the streamer-to-spark transition (Figure 11b). At higher air density at lower altitudes, the gas dynamics effect becomes pronounced much earlier during the transition (Figure 11a).

[35] Figure 12 shows τ_{br} at 0, 30, 50 and 70 km altitudes for the reduced field range $16 < EN_0/N < 24$ kV/cm. We emphasize that Figures 12a and 12b show the same exact values τ_{br} using different ways of scaling them with N . Figure 12a presents the results assuming that the transition times scale similarly to the vibrational-translational relaxation time (i.e., $\propto 1/N$) and Figure 12b presents the results assuming that the breakdown times scale similarly to the Joule heating timescale (i.e., $\propto 1/N^2$ [e.g., Achat *et al.*, 1992]).

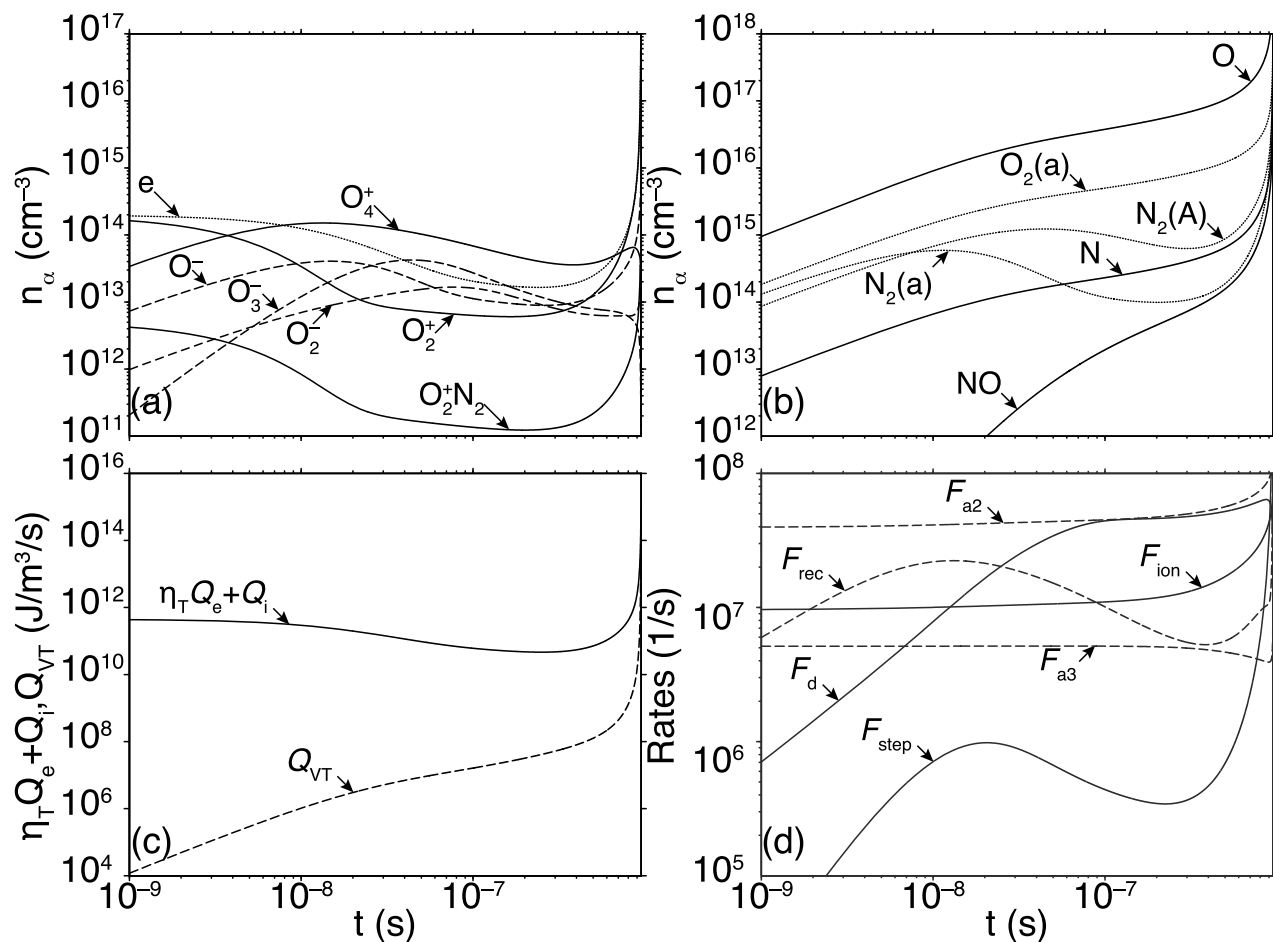


Figure 7. Temporal dynamics of the streamer-to-spark transition at altitude 0 km and $EN_0/N = 19$ kV/cm (continued from Figure 6). (a) Densities of charged species (e , O^- , O_2^- , O_3^- , O_2^+ , O_4^+ , and $O_2^+N_2$) and (b) densities of neutral species (O , N , NO , $O_2(a^1\Delta_g)$, $N_2(A^3\Sigma_u^+)$, and $N_2(a^1\Sigma_u^+)$) at the axis of the discharge. (c) Contributions from the fast heating ($\eta_T Q_e = \eta_T \sigma_e E^2$), ionic Joule heating ($Q_i = \sigma_i^0 E^2$), and vibrational-translational relaxation energy transfer (Q_{VT} expressed in $J m^{-3} s^{-1}$) appearing on the right side of the equation for translational energy (equation (5)). (d) Rates of generation and loss of electrons as a function of time.

The curves shown in Figures 12a and 12b would coincide if the heating followed the vibrational-translational or the Joule heating similarity laws, respectively. Therefore, the results shown in Figure 12b indicate a significant acceleration of the heating with reduction of air pressure. Figures 12a and 12b demonstrate that τ_{br} scales closer to $\propto 1/N$ than to $\propto 1/N^2$. This result agrees with conclusions reached in Figure 6 of Naidis [2005].

4. Discussion

[36] The model introduced in section 2, whose results are presented in section 3, allows us to investigate the influence of the treatment of positive ions in the kinetics scheme on the streamer-to-spark transition. It also permits us to quantitatively evaluate the scaling properties of the streamer-to-spark transition time. In this section, we discuss related questions and analyze the sensitivity of the model to the different employed approximations.

4.1. Comparison With Experimental Data and Approximations of Constant Pressure and Gas Density

[37] The timescales of streamer-to-spark transition are compared with the experimental measurements in Figure 4. The model results appear to be in excellent agreement with the experimental data under both normal and reduced pressure conditions (10^5 Pa and 0.75×10^5 Pa, respectively). In comparison, numerical modeling does not fit experimental data under the conditions of Joule heating assuming constant neutral density and constant conductivity of the channel (dashed line in Figure 4). The comparison of theoretical and experimental curves (solid lines and squares, open circles, and solid circles) with each other and with the results obtained for the Joule heated channel at constant density and channel conductivity, therefore, emphasizes the necessity of including the time-dependent chemical kinetics and partitioning of energy between fast heating and vibrational excitation in order to reproduce the experimentally observed results (see Figure 4).

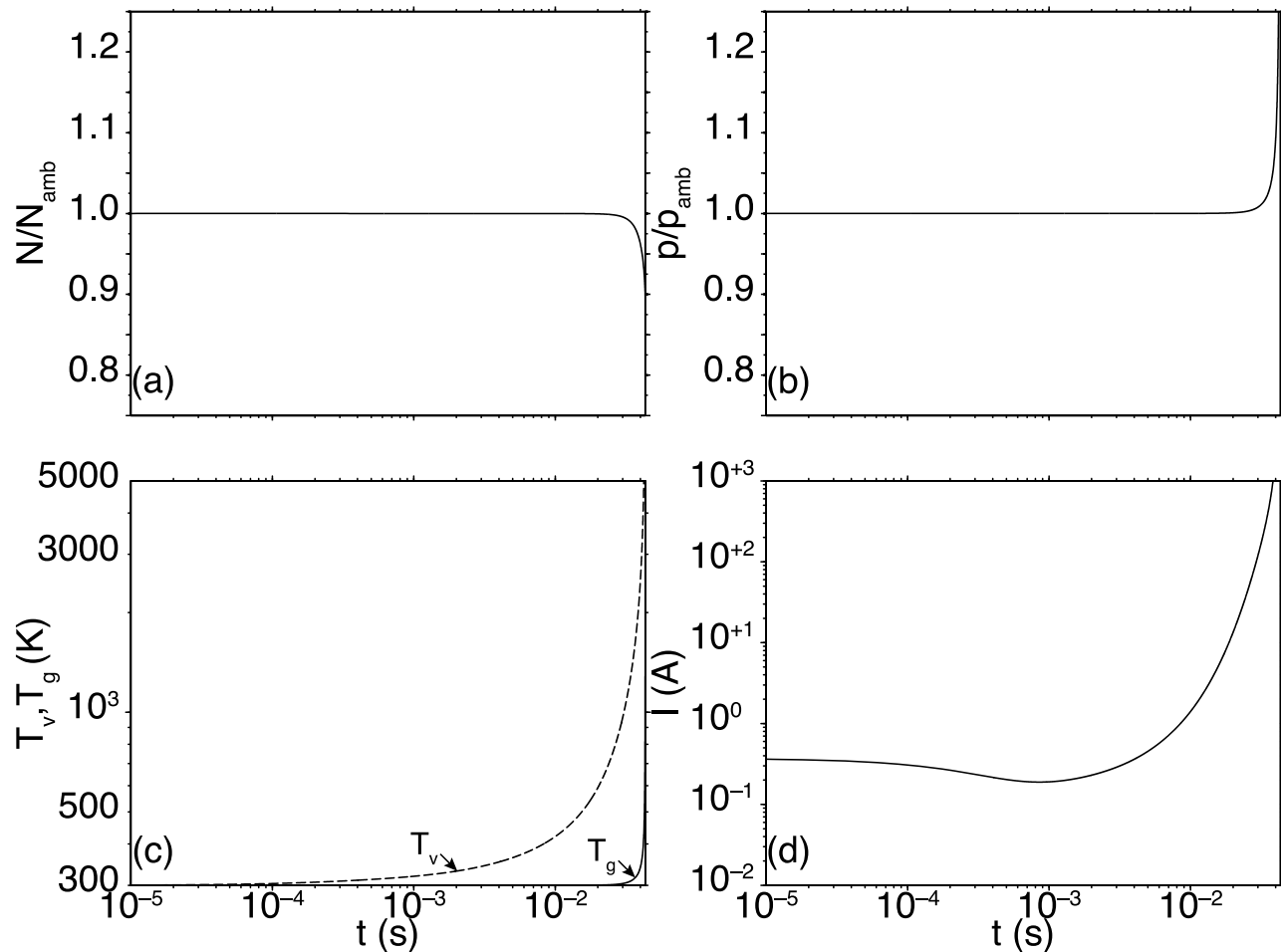


Figure 8. (a–d) Same as in Figure 6 but for temporal dynamics of the streamer-to-spark transition at altitude 70 km and $EN_0/N = 19$ kV/cm.

[38] At low-applied voltage, the gas dynamics, which leads to the expansion of the channel and to the reduction of the air density N , plays a dominant role. Under these conditions the pressure p stays approximately constant with the increase in the gas temperature T_g . Low-applied voltages correspond to longer breakdown times allowing the pressure to be equalized on the timescale of the streamer-to-spark transition, i.e., allowing us to make the assumption that the channel remains under constant pressure. The high-applied voltages lead to very small τ_{br} such that $\tau_{\text{br}} \ll r_s/c_s$, allowing us to assume that the neutral density barely varies during the time of the transition. Therefore, it is expected that the 1-D model (including the gas dynamics) converges toward the 0-D model under assumption of constant pressure at lower-applied voltage, and toward the 0-D model under constant density for higher-applied voltage (Figure 5), consistent with previous results by *Naidis* [2005]. In the latter case, the transition occurs too fast to allow the gas dynamics to play any significant role. From this result, it follows that the effects of the gas dynamics can be neglected at high-reduced electric field E/N , i.e., when the timescale of the variation of the neutral gas density is too slow to compete with that of the kinetics effects. When the neutral gas density varies on a timescale comparable to that of the streamer-to-spark transition, the gas dynamics effects act in parallel with the

kinetics mechanisms and increase the ionization (through an increase of the reduced electric field), resulting in a faster transition. Consequently, the gas dynamics is able to accelerate the transition to spark at low-applied voltage.

[39] Another interesting fact in Figure 5 lies in the differences of the transition times between 0-D constant density and constant pressure models at 0 and 70 km. At ground level, they can differ by a factor ~ 2 to 3, but at higher altitude, their difference does not exceed $\sim 25\%$ as evidenced by Figure 5. Figure 6c shows that at high air density, the temperature increases steadily throughout most of the duration of the transition (until $t = 0.5 \mu\text{s}$) and then increases exponentially. Therefore, the variations of T_g are too large to be negligible in this case, and the pressure p cannot be assumed to be simply proportional to the air density N ($p \propto N$) (see Figures 6a and 6b). Hence, the 0-D models under assumptions of constant pressure or density differ significantly for any applied electric field and for both kinetic models (Figures 5a and 5b). At higher altitude (Figures 5c and 5d), the gas temperature remains almost constant until the very last stages of the transition when it rapidly increases exponentially (Figure 8c). Hence, both the pressure and air density remain quasi-constant (see Figures 8a and 8b) and such that effectively $p \propto N$ most of the time. Consequently there is little difference between the two 0-D models as observed in Figures 5c and

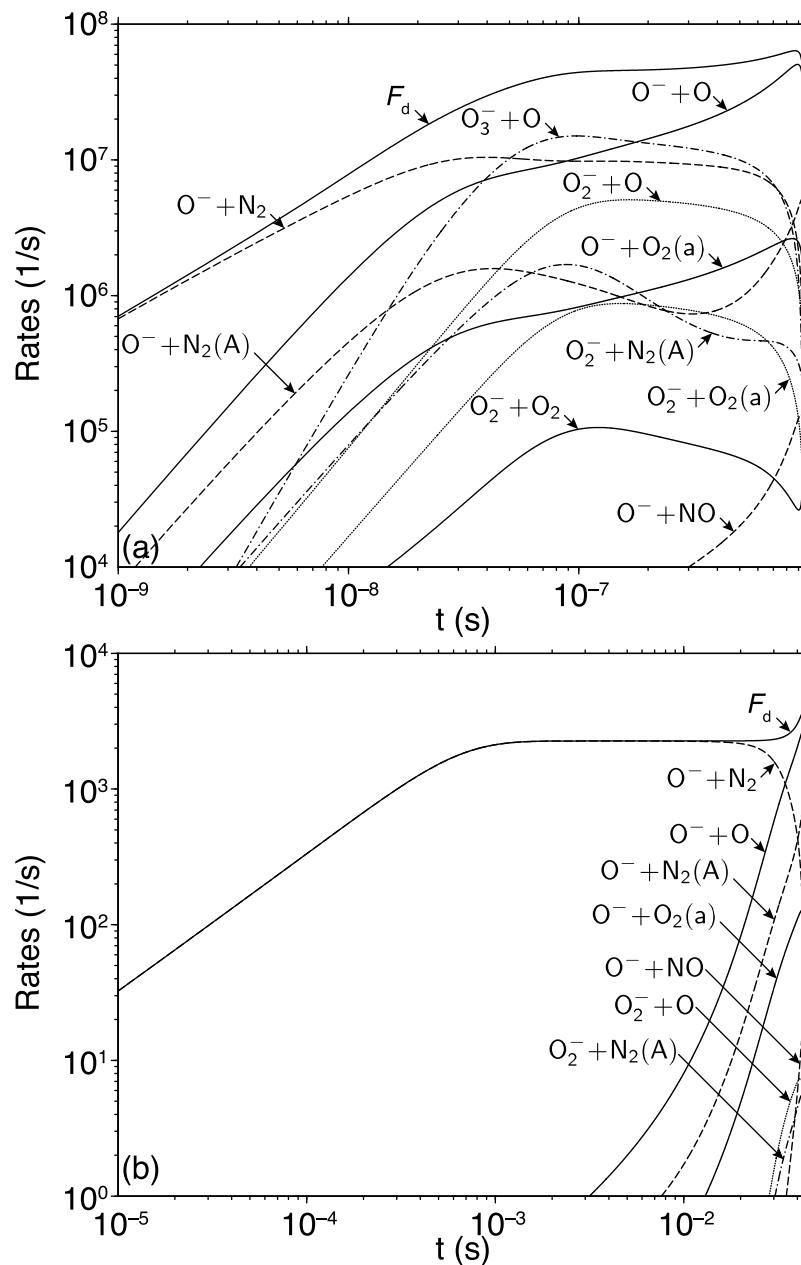


Figure 10. Contributions of all reactions of detachment (R13–R22 in Table 2) to the total detachment rate F_d throughout the duration of the streamer-to-spark transition at (a) 0 and (b) 70 km.

10^8 cm^{-3} and $n_{\text{NO}} \simeq 1.2 \times 10^7 \text{ cm}^{-3}$ [e.g., *Sentman et al.* 2008a, Table 2]. Whether these initial densities are introduced in the model or not does not produce any noticeable change in the time of streamer-to-spark transition for applied $EN_0/N = 14\text{--}24 \text{ kV/cm}$, and altitude range between 0 and 70 km. The initial densities of O_3 and NO are maintained to their initial values until the last stages of the transition, when the behavior of n_{O_3} and n_{NO} with nonzero initial conditions closely follow the dynamics of these species with zero initial densities. The study of the dynamics of O_3 requires to include reactions of production and destruction of O_3 . Based on the estimations of the timescales of several reactions of production and destruction of O_3 , it can be shown that O_3 is primarily produced by collisions of atomic oxygen with O_2 in the

reaction: $\text{O} + \text{O}_2 + \text{O}_2 \rightarrow \text{O}_2 + \text{O}_3$ (with constant of reaction $k_f = 8.6 \times 10^{-31} T_g[\text{K}]^{-1.25} \text{ cm}^6 \cdot \text{s}^{-1}$) and destroyed in the reaction $\text{O}_2 + \text{O}_3 \rightarrow \text{O} + \text{O}_2 + \text{O}_2$ (with constant of reaction $k_d = 73 \times 10^{-11} e^{-11400/T_g[\text{K}]} \text{ cm}^3 \cdot \text{s}^{-1}$) [*Parissi et al.*, 2000]. *Parissi et al.* [2000] emphasized that the dependence of k_f and k_d on the temperature T_g implies that the ozone destruction reaction is favored for high temperature. Using $n_{\text{O}_3} \simeq 6 \times 10^8 \text{ cm}^{-3}$ [*Sentman et al.*, 2008a] and $n_{\text{O}} \simeq 2 \times 10^{10} \text{ cm}^{-3}$ [e.g., *Harlow and Riehl*, 1991] for the initial concentrations in O_3 and O at 70 km, our simulation results demonstrate that destruction of O_3 is favored for gas temperature above $\sim 600 \text{ K}$. If the initial temperature is high enough, then we observe a destruction of the initially present O_3 molecules, in agreement with the above discussion.

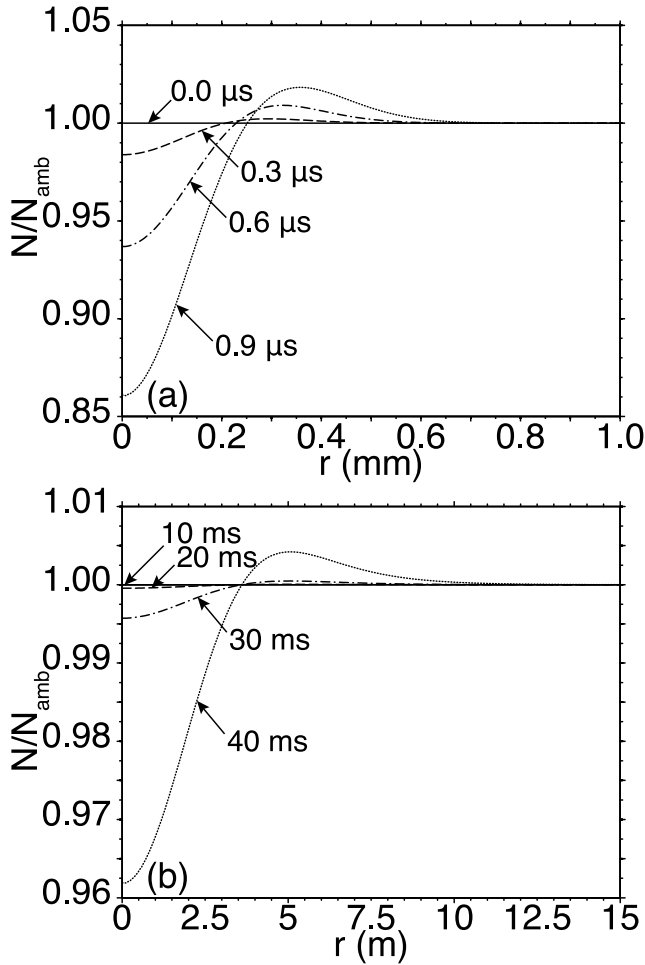


Figure 11. Distribution of the normalized air density as a function of the radial coordinate (a) at 0 km at $t = 0, 0.3, 0.6,$ and $0.9 \mu\text{s}$ and (b) at 70 km at $t = 10, 20, 30,$ and 40 ms .

[44] Similarly, if the ambient density of atomic oxygen at 70 km is accounted for ($n_{\text{O}} \simeq 2 \times 10^{10} \text{ cm}^{-3}$ [e.g., Harlow and Riehl, 1991]), then the number density of O remains close to its initial value until the last stages of the transition, when the difference between the dynamics of atomic oxygen with and without the initial ambient density of O is no longer significant. Quantitatively, the addition of the initial n_{O} density produces a small acceleration of the streamer-to-spark transition by decreasing the breakdown times by $\lesssim 1\%$ for applied $EN/N_0 = 14\text{--}24 \text{ kV/cm}$.

[45] The concentration of CO_2 molecules at 70 km in the Earth atmosphere is on the order of $5 \times 10^{11} \text{ cm}^{-3}$ [e.g., Sentman et al., 2008a] and nonradiating vibrationally excited $\text{N}_2(\text{v})$ molecules are expected to efficiently transfer their energy to $\text{CO}_2(\nu_3)$ vibrational states that then radiate infrared emissions at $4.3 \mu\text{m}$ [e.g., Kumer, 1977; Picard et al., 1997, and references therein]. The transfer of vibrational energy from N_2 to CO_2 takes from several seconds at 70 km to a minute at 90 km altitude [e.g., Picard et al., 1997]. Although the lifetime of $\text{CO}_2(\nu_3)$ is very short ($\sim 2 \text{ ms}$), in the mesosphere the effective lifetime of $\text{CO}_2(\nu_3)$ and relaxation time of $\text{N}_2(\text{v})$ are both lengthened considerably by reabsorption of $4.3 \mu\text{m}$ photons (radiation trapping) and by the reverse VV process in which the vibrational energy is passed back to N_2 .

The effective relaxation times of $\text{N}_2(\text{v})$ are in the range of 5–7 min at 70–90 km altitude [Kumer, 1977; Picard et al., 1997]. These timescales exceed by several orders of magnitude the heating timescales reported in the present work and, therefore, related processes are not included in the present model.

4.5. Effects of Positive Ion Chemistry

[46] The comparison of Figures 5a and 5b emphasizes the effects of different positive ions included in the model. For the simulation results presented in this work, N_2^+ and N_4^+ ions are readily converted into O_2^+ ions [e.g., Naidis, 1999]. This hypothesis has been tested and simulation results (not presented here for the sake of brevity) have shown that nitrogen positive ions remain in negligible quantity at any moment of the simulation at any altitude. The densities of the positive ions in Figures 7a and 9a reveal that O_4^+ is the dominant ion at low altitude, and O_2^+ is the main positive ion at high altitude. The O_4^+ ion is produced in a three-body processes R58 and is lost in two-body processes (R11, R48, R51, R54, R56, R57, R61, and R63). The O_2^+N_2 ion is produced in the three-body process R60 and can lead to O_4^+ ion via a two-body reaction

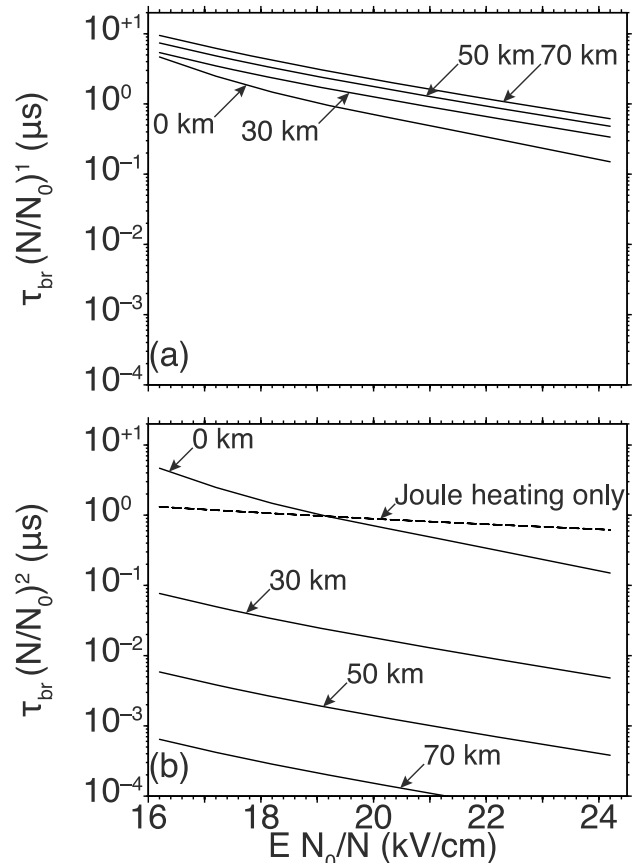


Figure 12. Scaling of the breakdown times as a function of the air density for various applied electric fields and altitudes (0, 30, 50, and 70 km): (a) $\tau_{\text{br}} \propto 1/N$, the scaling is the same as that of the vibrational-translational relaxation timescale and (b) $\tau_{\text{br}} \propto 1/N^2$, the scaling is the same as that of the Joule heating timescale, assuming constant air density N and time-independent conductivity of the channel.

R59. Therefore, the production of both O_4^+ and $O_2^+N_2$ ions fundamentally occurs in three-body interactions. The O_2^+ ion is produced in direct electron impact ionization (R1) and in charge transfer reactions involving N_2^+ and N_4^+ ions [e.g., *Sentman et al.*, 2008a, 2008b] that are two-body processes. The O_2^+ ion is lost in both two-body processes (R9, R44–R47, R50, and R53) and three-body processes (R10, R58, and R60). The decrease of neutral density with altitude reduces the importance of three-body processes compared with two-body processes (as evidenced, in particular, in Figures 7d and 9d for two- and three-body attachment), and makes O_2^+ the dominant positive ion at higher altitude (see Figure 9a).

[47] Our model results indicate that whether or not positive ions O_4^+ and $O_2^+N_2$ are explicitly included in the model has direct consequences on the streamer-to-spark transition time. In particular, as already emphasized in section 3, at ground conditions the transition into spark is significantly longer when O_4^+ and $O_2^+N_2$ ions are taken into account (see Figures 5a and 5b), mainly due to the fast recombination of electrons with these ions and resultant reduction in electron conductivity. At higher altitude, there is no noticeable difference between the kinetics schemes including O_2^+ only or the full O_2^+ , O_4^+ , and $O_2^+N_2$ positive ion chemistry (Figures 5c and 5d, respectively). Indeed, Figure 9a shows that even when O_4^+ and $O_2^+N_2$ are accounted for in the kinetics scheme, they are negligible at all times during the transition in comparison with O_2^+ ions.

[48] The refined treatment of the chemistry of the plasma including O_4^+ and $O_2^+N_2$ is expected to improve the accuracy of the results, yet it involves reactions of ion-ion recombinations, whose rates are still poorly known. The works by *Kossyi et al.* [1992] and *Sentman et al.* [2008a, 2008b] provide a significant number of reactions of ion-ion recombination, but their lists are not exhaustive, as for example the recombinations of complex ions such as O_4^+ with O^- are not included.

[49] The kinetic scheme presented in the present paper does not include three-body ion-ion recombination reactions (for example, reactions (V) and (VI) of *Kossyi et al.* [1992]). If three-body ion-ion recombinations were included, then the number of unknown rates of reactions would increase significantly and, therefore, would introduce an additional source of uncertainty. We restrain the reactions of ion-ion recombination in the kinetic scheme to well-documented two-body reactions (R44–R55 in Table 2). *Benilov and Naidis* [2003] even further simplified the treatment of ion-ion interactions in their model by treating all ion-ion recombinations through a unique reaction denoted $X^+ + Y^- \rightarrow X + Y$, where X^+ and Y^- represent any positive and negative ions, respectively.

4.6. Role of Ion Temperature

[50] *Naidis* [1999] and G. V. Naidis (private communication, 2010) suggests that the reaction rates of the interaction between positive ions and neutral particles (R56–R63 in Table 2) should depend on the effective temperatures of positive ions colliding with N_2 and O_2 molecules, denoted $T_{N_2,eff}^+$ and $T_{O_2,eff}^+$, respectively. In this section, we illustrate the effects of ion temperatures on the positive ion composition and dynamics of streamer-to-spark transition. The temperatures $T_{N_2,eff}^+$ and $T_{O_2,eff}^+$ are defined as $T_{N_2,eff}^+ = (m_+T_g + m_{N_2}T_{N_2}^+)/ (m_+ + m_{N_2})$ and $T_{O_2,eff}^+ = (m_+T_g + m_{O_2}T_{O_2}^+)/ (m_+ + m_{O_2})$

[*Naidis*, 1999], and m_+ , m_{N_2} , and m_{O_2} refer to the masses of the positive ions (O_2^+ , O_4^+ , or $O_2^+N_2$) and N_2 and O_2 molecules, respectively (see Table 1), and T_{N_2,O_2}^+ is the temperature of positive ions colliding with N_2 and O_2 : $T_{N_2,O_2}^+ = T_g + (m_+ + m_{N_2,O_2})(\mu_+E)^2/(3k_B)$ [*Mnatsakanyan and Naidis*, 1991]. If $T_{N_2,eff}^+$ is substituted in place of T_g in R61, R62, and R63, and $T_{O_2,eff}^+$ in place of T_g in R58 and R60, then changes on the breakdown times $\tau_{br} \lesssim 25\%$ are observed at 0 km for $EN/N_0 = 14$ – 24 kV/cm, and no noticeable change in τ_{br} is reported at 70 km for $EN/N_0 = 14$ – 24 kV/cm, where the concentrations of O_4^+ and $O_2^+N_2$ ions are small. The significant increases of the rates of reactions R61–R63 at 0 km favor the conversion of O_4^+ into O_2^+ , making O_2^+ the dominant ion for all the range of studied applied reduced electric fields and altitudes (see Figure 13), consistent with the results reported by *Naidis* [1999].

4.7. Role of Associative Ionization Reactions

[51] *Popov* [2003] emphasizes the role of the reactions of associative ionization (R4 and R5 in Table 2) in the explosive increase in the electron density leading to the transition to spark. The comparisons of breakdown times τ_{br} produced by our model for $EN_0/N = 14$ – 24 kV/cm at 0 and 70 km altitude show that ignoring these reactions would affect the transition time most significantly at high-reduced electric field E/N . For $EN_0/N = 14$ kV/cm, τ_{br} increases by a few percents ($<2\%$) if R4 and R5 are neglected, because the timescales of the reactions of associative ionization ($\tau_{R4-R5} \gtrsim 50 \mu s$ at 0 km and $\tau_{R4-R5} \gtrsim 10$ s at 70 km) are longer than the streamer-to-spark transition times ($\tau_{br} = 26.7 \mu s$ at 0 km and $\tau_{br} = 0.37$ s at 70 km). At higher-reduced fields, for $EN_0/N = 24$ kV/cm the timescales of the reactions R4 and R5 are on the order of 0.1–1 μs and $\gtrsim 1$ s at 0 and at 70 km altitudes, respectively. These timescales are comparable with the streamer-to-spark transition time, suggesting a significant effect of the reactions of associative ionization on the dynamics of the transition under these conditions. This observation is confirmed by the model results, which show that in the absence of R4 and R5, the breakdown time is delayed by up to $\sim 40\%$ at 0 km altitude for $EN_0/N = 24$ kV/cm, when $\tau_{R4-R5} \ll \tau_{br}$.

4.8. Scaling of Heating Time With Air Density and Thermal Conduction and Diffusion Losses

[52] The effective timescale of the cooling of the streamer channel due to the thermal conduction effects scales with ambient air density as $1/N$, and previous studies have established that the effective Joule heating time in streamer channels under conditions of constant channel conductivity and air density scales as $1/N^2$, therefore, leading to a better heat confinement and an easier transition to spark at higher gas pressures in comparison with low pressures [*Achat et al.*, 1992].

[53] Because the adjusted heating time scaling factor for the breakdown time ($\tau_{br} \propto 1/N^{1.11}$) lies between the scaling factor of the vibrational-translational relaxation ($\propto 1/N$) and that of the Joule heating timescale ($\propto 1/N^2$), our results and those in Figure 6 of *Naidis* [2005] demonstrate that kinetic effects lead to a significant acceleration of the heating, with effective heating times appearing to scale closer to $1/N$ than to $1/N^2$, which is predicted on the basis of simple similarity laws for Joule heating [*Achat et al.*, 1992].

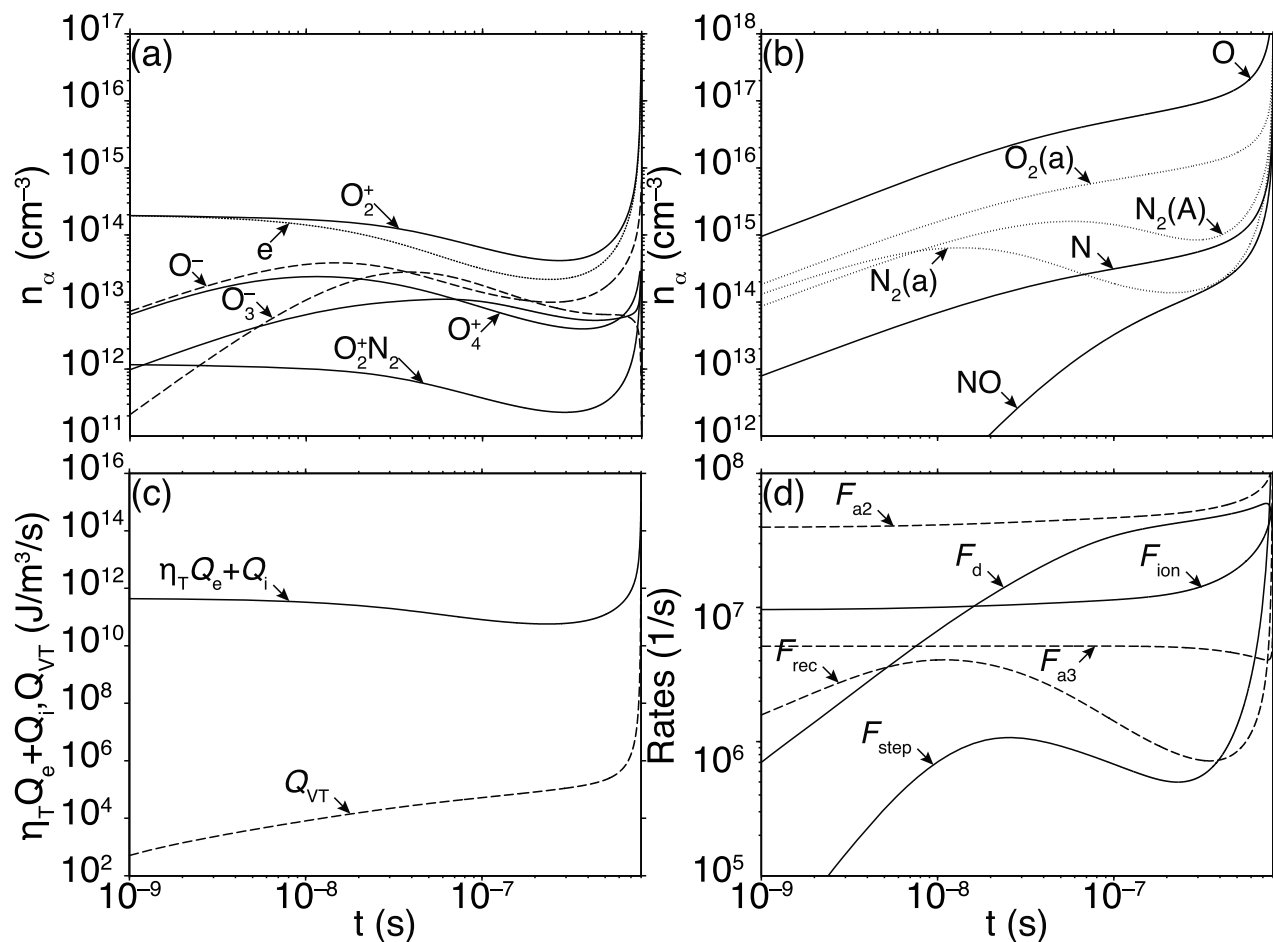


Figure 13. Temporal dynamics of the streamer-to-spark transition at altitude 0 km and $EN_0/N = 19$ kV/cm, accounting for the effective temperature of positive ions as suggested by *Naidis* [1999]. (a–d) Same as in Figure 6 but for the case $\tau_{br} = 0.8 \mu\text{s}$.

[54] These results have significant consequences for the evaluation of the importance of different processes for gas heating in streamer channels at low gas pressures. Specifically, they imply that all the processes, which have effective times that scale proportionally to $1/N$, which are determined to be unimportant for streamer-to-spark transition at ground pressure can still be ignored at lower pressures. These processes include, in particular, the thermal conduction processes, which lead to the cooling of the streamer channel [*Achat et al.*, 1992; *Tardiveau et al.*, 2001], the diffusion of charged and neutral species [*Naidis*, 2005] and losses related to the radial drift of ions [*Naidis*, 2005]. In the same vein it is important to emphasize that the vibrational-translational relaxation time τ_{VT} scales as $1/N$ and since heating time also scales close to $1/N$ there is no significant acceleration of the heating due to transfer of vibrational energy from N_2 molecules, as would be expected if heating time scaled as $1/N^2$.

5. Conclusions

[55] In this paper, an air-density-dependent model of streamer-to-spark transition is introduced. The model allows investigation of effective timescales τ_{br} of the initial stage of air heating in streamer channels up to 5000 K at which the

thermal ionization becomes important. It accounts for the effects of the dynamic expansion of the heated air on the reduced electric field E/N and of the resultant plasma kinetics in the streamer channel. It also includes the transfer of energy through vibrational-translational relaxation of N_2 molecules, and a realistic partition of input energy into gas heating and vibrational excitation of N_2 molecules during the streamer-to-spark transition dynamics. In addition to ionization kinetics, involving the production and interaction of electrons and different types of positive and negative ions, the model accounts for self quenching of $N_2(A^3\Sigma_u^+)$ excited molecules, and associative ionization processes involving $N_2(A^3\Sigma_u^+)$ and $N_2(a^1\Sigma_u^-)$ species. The model also accounts for the effects of gains in electron energy in collisions with vibrationally excited $N_2(v)$ on the rate constants of processes involving electron impact collisions. The model self-consistently couples a fully 1-D axisymmetric, axially invariant gas dynamics model to a 0-D kinetics scheme involving 17 species in more than 60 reactions through the derivation of the Joule heating and of the related energy participating in the channel. The model results are successfully compared with experimental data obtained by *Černák et al.* [1995] and *Larsson* [1998] at ground and near-ground pressure. The model results confirm the previous results by other authors obtained at ground

pressure that the fast release of electrons in detachment collisions is a critically important process for fast gas heating in streamer channels during the streamer-to-spark transition. Classic 0-D models under assumptions of constant gas density or constant pressure, and the 1-D model are also compared, and it is shown that the three models lead to similar results at lower air density (i.e., at high altitudes), but differ significantly at higher air density. The results indicate that at low ambient air densities the channel conductivity and the air temperature increase very rapidly in comparison with gas dynamic expansion time (i.e., $\tau_{br} \leq r_s/c_s$, where r_s is the streamer channel radius and c_s is speed of sound) so both constant density and constant pressure approximations to channel dynamics commonly used in previous studies at ground pressure lead to nearly identical streamer-to-spark transition times. It is shown that at lower-applied electric field, the 1-D model (including the gas dynamics) converges toward the 0-D model under the assumption of constant pressure while for higher-applied electric field it converges toward the 0-D model under constant density. At ground and near-ground pressure, these results are in excellent agreement with the prior results on this topic reported by Naidis [2005]. The present work demonstrates that for a broad range of air densities studied (between altitudes 0 and 70 km), the streamer-to-spark transition time scales with neutral density as: $\tau_{br} \propto N^{-1.11}$, i.e., faster than the timescale of Joule heating assuming constant air density and conductivity in the streamer channel ($\propto N^{-2}$) but slower than that of the vibrational-translational relaxation ($\propto N^{-1}$). The obtained model heating times for the altitude range indicate substantial relative (i.e., scaled with $1/N^2$) acceleration of the air heating, when compared with the ground level. This acceleration is attributed to strong reduction in electron losses due to three-body attachment and electron-ion recombination with reduction of air pressure. The vibrational-translational relaxation time τ_{VT} scales as $1/N$ and since heating time also scales close to $1/N$ there is no significant acceleration of the heating due to transfer of vibrational energy from N_2 molecules, as would be expected if heating time scaled as $1/N^2$.

[56] **Acknowledgments.** The authors gratefully acknowledge discussions with D. D. Sentman, E. Marode, G. Naidis, C. O. Laux, and L. Caillaud. The authors also thank N. Liu for his valuable input on the development of the algorithms for the calculation of the partition of energy between fast gas heating and vibrational excitation of N_2 molecules. This research was supported by the NSF under grant AGS-0652148 to Pennsylvania State University.

[57] Bob Lysak thanks George Naidis and an anonymous reviewer for their assistance in evaluating this paper.

References

- Achat, S., Y. Teisseyre, and E. Marode (1992), The scaling of the streamer-to-arc transition in a positive point-to-plane gap with pressure, *J. Phys. D Appl. Phys.*, *25*(4), 661–668.
- Akshchev, Y. S., G. I. Aponin, M. E. Grushin, V. B. Karal'nik, A. E. Monich, M. V. Pan'kin, and N. I. Trushkin (2007), Development of a spark sustained by charging the stray capacitance of the external circuit in atmospheric-pressure nitrogen, *Plasma Phys. Rep.*, *33*(7), 584–601, doi:10.1134/S1063780X07070082.
- Aleksandrov, N. L., and E. M. Bazelyan (1999), Ionization processes in spark discharge plasmas, *Plasma Sources Sci. Technol.*, *8*(2), 285–294.
- Aleksandrov, N. L., A. E. Bazelyan, E. M. Bazelyan, and I. V. Kochetov (1995), Modeling of long streamers in atmospheric-pressure air, *Plasma Phys. Rep.*, *21*(60), 57–75.
- Aleksandrov, N. L., E. M. Bazelyan, I. V. Kochetov, and N. A. Dyatko (1997), The ionization kinetics and electric field in the leader channel in long air gaps, *J. Phys. D Appl. Phys.*, *30*(11), 1616–1624, doi:10.1088/0022-3727/30/11/011.
- Aleksandrov, N. L., E. Bazelyan, N. Dyatko, and I. Kochetov (1998), Streamer breakdown of long air gaps, *Plasma Phys. Rep.*, *24*(7), 541–555.
- Aleksandrov, N. L., E. M. Bazelyan, and A. M. Konchakov (2001), Plasma parameters in the channel of a long leader in air, *Plasma Phys. Rep.*, *27*(10), 875–885.
- Bastien, F., and E. Marode (1985), Breakdown simulation of electro-negative gases in non-uniform field, *J. Appl. Phys.*, *18*(3), 377–393.
- Bazelyan, E. M., and Y. P. Raizer (1998), *Spark Discharge*, 294 pp., Chem. Rubber, New York.
- Bazelyan, E. M., Y. P. Raizer, and N. L. Aleksandrov (2007), The effect of reduced air density on streamer-to-leader transition and on properties of long positive leader, *J. Phys. D Appl. Phys.*, *40*(14), 4133–4144.
- Benilov, M. S., and G. V. Naidis (2003), Modelling of low-current discharges in atmospheric-pressure air taking account of non-equilibrium effects, *J. Phys. D Appl. Phys.*, *36*(15), 1834–1841, doi:10.1088/0022-3727/36/15/314.
- Benilov, M. S., and G. V. Naidis (2005), Modelling of discharges in a flow of preheated air, *Plasma Sources Sci. Technol.*, *14*(1), 129–133, doi:10.1088/0963-0252/14/1/015.
- Brown, R. A. (1991), *Fluid Mechanics of the Atmosphere*, *Int. Geophys. Ser.*, vol. 47, 2nd ed., 489 pp., Academic, San Diego, Calif.
- Černák, M., E. M. van Veldhuizen, I. Morva, and W. R. Rutgers (1995), Effect of cathode surface properties on glow-to-arc transition in a short positive corona gap in ambient air, *J. Phys. D Appl. Phys.*, *28*(6), 1126–1132.
- Comtois, D., et al. (2003), Triggering and guiding of an upward positive leader from a ground rod with an ultrashort laser pulse—Part II: Modeling, *IEEE Trans. Plasma Sci.*, *31*(3), 387–395, doi:10.1109/TPS.2003.811649.
- Courant, R., K. Friedrichs, and H. Lewy (1928), Partial differential equations of mathematical physics, *Math. Ann.*, *100*, 32–74.
- Cummer, S. A., J. B. Li, F. Han, G. P. Lu, N. Jaugey, W. A. Lyons, and T. E. Nelson (2009), Quantification of the troposphere-to-ionosphere charge transfer in a gigantic jet, *Nat. Geosci.*, *2*(9), 617–620, doi:10.1038/ngeo607.
- De Larquier, S. (2010), Finite-difference time-domain modeling of infrasound propagation in a realistic atmosphere, M.S. thesis, Pa. State Univ., University Park, Pa.
- Farges, T. (2009), Infrasound from lightning and sprites, in *Lightning: Principles, Instruments and Applications: Review of Modern Lightning Research*, edited by H. D. Betz, U. Schumann, and P. Laroche, chap. 18, pp. 417–432, Springer, New York.
- Farges, T., and E. Blanc (2010), Characteristics of infrasound from lightning and sprites near thunderstorm areas, *J. Geophys. Res.*, *115*, A00E31, doi:10.1029/2009JA014700.
- Farges, T., E. Blanc, A. L. Pichon, T. Neubert, and T. H. Allin (2005), Identification of infrasound produced by sprites during the Sprite2003 campaign, *Geophys. Res. Lett.*, *32*, L01813, doi:10.1029/2004GL021212.
- Flitti, A., and S. Pancheshnyi (2009), Gas heating in fast pulsed discharges in N_2 - O_2 mixtures, *Eur. Phys. J. Appl. Phys.*, *45*(2), 21001, doi:10.1051/epjap/2009011.
- Gallimberti, I. (1979), The mechanism of the long spark formation, *J. Phys. Coll.*, *40*(C7), 193–250.
- Gallimberti, I., G. Bacchiega, A. Bondiou-Clergerie, and P. Lalande (2002), Fundamental processes in long air gap discharges, *C. R. Phys.*, *3*(10), 1335–1359, doi:10.1016/S1631-0705(02)01414-7.
- Gordillo-Vázquez, F. J. (2008), Air plasma kinetics under the influence of sprites, *J. Phys. D Appl. Phys.*, *41*(23), 234016, doi:10.1088/0022-3727/41/23/234016.
- Hagelaar, G. J. M., and L. C. Pitchford (2005), Solving the Boltzmann equation to obtain electron transport coefficients and rate coefficients for fluid models, *Plasma Sources Sci. Technol.*, *14*(4), 722–733.
- Harlow, H. B., and J. P. Riehl (1991), Recovery of atomic oxygen density and temperature of the thermosphere by numerical inversion of simulated infrared radiance data with Gaussian noise, *Planet. Space Sci.*, *39*(8), 1155–1162, doi:10.1016/0032-0633(91)90167-9.
- Kossyi, I. A., A. Y. Kostinsky, A. A. Matveyev, and V. P. Silakov (1992), Kinetic scheme of the non-equilibrium discharge in nitrogen-oxygen mixtures, *Plasma Sources Sci. Technol.*, *1*(3), 207–220.
- Krehbiel, P. R., J. A. Riousset, V. P. Pasko, R. J. Thomas, W. Rison, M. A. Stanley, and H. E. Edens (2008), Upward electrical discharges from thunderstorms, *Nat. Geosci.*, *1*(4), 233–237, doi:10.1038/ngeo162.
- Kumer, J. (1977), Theory of CO_2 4.3- μ m-aurora and related phenomena, *J. Geophys. Res.*, *82*(16), 2203–2209.
- Larsson, A. (1998), The effect of a large series resistance on the streamer-to-spark transition in dry air, *J. Phys. D Appl. Phys.*, *31*(9), 1100–1108.

- Liszka, L., and Y. Hobara (2006), Sprite-attributed infrasonic chirps—Their detection, occurrence and properties between 1994 and 2004, *J. Atmos. Sol. Terr. Phys.*, *68*(11), 1179–1188.
- Liu, N. Y., and V. P. Pasko (2004), Effects of photoionization on propagation and branching of positive and negative streamers in sprites, *J. Geophys. Res.*, *109*, A04301, doi:10.1029/2003JA010064.
- Liu, N. Y., V. P. Pasko, K. Adams, H. C. Stenbaek-Nielsen, and M. G. McHarg (2009), Comparison of acceleration, expansion, and brightness of sprite streamers obtained from modeling and high-speed video observations, *J. Geophys. Res.*, *114*, A00E03, doi:10.1029/2008JA013720.
- Lowke, J. J. (1992), Theory of electrical breakdown in air—The role of metastable oxygen molecules, *J. Phys. D Appl. Phys.*, *25*(2), 202–210.
- Marode, E. (1983), The glow-to-arc transition, in *Electrical Breakdown and Discharges in Gases: Macroscopic Processes and Discharges*, vol. B, edited by E. E. Kunhardt and L. H. Luessen, pp. 119–166, Plenum Press, New York.
- Marode, E., F. Bastien, and M. Bakker (1979), Model of the streamer-induced spark formation based on neutral dynamics, *J. Atmos. Terr. Phys.*, *50*(1), 140–146.
- Mnatsakanyan, A. K., and G. V. Naidis (1985), The vibrational-energy balance in a discharge in air, *High Temp.*, *23*(4), 506–513.
- Mnatsakanyan, A. K., and G. V. Naidis (1991), Charged particle production and loss processes in nitrogen–oxygen plasmas, in *Reviews of Plasma Chemistry*, vol. 1, edited by B. M. Smirnov, Consult. Bur., New York.
- Morrow, R., and J. J. Lowke (1997), Streamer propagation in air, *J. Phys. D Appl. Phys.*, *30*(4), 614–627.
- Naidis, G. V. (1999), Simulation of streamer-to-spark transition in short non-uniform air gaps, *J. Phys. D Appl. Phys.*, *32*(20), 2649–2654.
- Naidis, G. V. (2005), Dynamics of streamer breakdown of short non-uniform air gaps, *J. Phys. D Appl. Phys.*, *38*(21), 3889–3893.
- Naidis, G. V. (2007), Simulation of convection-stabilized low-current glow and arc discharges in atmospheric-pressure air, *Plasma Sources Sci. Technol.*, *16*(2), 297–303, doi:10.1088/0963-0252/16/2/012.
- Naidis, G. V. (2008), Simulation of spark discharges in high-pressure air sustained by repetitive high-voltage nanosecond pulses, *J. Phys. D Appl. Phys.*, *41*(23), 234017, doi:10.1088/0022-3727/41/23/234017.
- Naidis, G. V. (2009), Simulation of streamer-induced pulsed discharges in atmospheric-pressure air, *Eur. Phys. J. Appl. Phys.*, *47*(2), 22803, doi:10.1051/epjap/2009084.
- Parissi, L., E. Odic, A. Goldman, M. Goldman, and J.-P. Borra (2000), Temperature effects on plasma chemical reactions—Application to VOC removal from flue gases by dielectric-barrier discharges, in *Electrical Discharges for Environmental Purposes: Fundamentals and Applications*, edited by E. M. van Veldhuizen, chap. 11, pp. 279–313, Nova Sci., Huntington, N. Y.
- Pasko, V. P. (2006), Theoretical modeling of sprites and jets, in *Sprites, Elves and Intense Lightning Discharges*, NATO Sci. Ser. II, vol. 225, edited by M. Füllekrug, E. A. Mareev, and M. J. Rycroft, pp. 253–311, Springer, Heidelberg, Germany.
- Pasko, V. P., and J. J. George (2002), Three-dimensional modeling of blue jets and blue starters, *J. Geophys. Res.*, *107*(A12), 1458, doi:10.1029/2002JA009473.
- Pasko, V. P., and J. B. Snively (2007), Mechanism of infrasound radiation from sprites, *Eos Trans. AGU*, *88*(52), Fall Meet. Suppl., Abstract AE23A-0899.
- Pasko, V. P., U. S. Inan, and T. F. Bell (1998), Spatial structure of sprites, *Geophys. Res. Lett.*, *25*(12), 2123–2126.
- Pasko, V. P., M. A. Stanley, J. D. Matthews, U. S. Inan, and T. G. Wood (2002), Electrical discharge from a thundercloud top to the lower ionosphere, *Nature*, *416*(6877), 152–154, doi:10.1038/416152a.
- Petrov, N. I., and G. N. Petrova (1999), Physical mechanisms for the development of lightning discharges between a thundercloud and the ionosphere, *Tech. Phys. Lett.*, *44*(4), 472–475.
- Picard, R. H., U. S. Inan, V. P. Pasko, J. R. Winick, and P. P. Wintersteiner (1997), Infrared glow above thunderstorms?, *Geophys. Res. Lett.*, *24*(21), 2635–2638.
- Popov, N. A. (2001), Investigation of the mechanism for rapid heating of nitrogen and air in gas discharges, *Plasma Phys. Rep.*, *27*(10), 886–896, doi:10.1134/1.1409722.
- Popov, N. A. (2003), Formation and development of a leader channel in air, *Plasma Phys. Rep.*, *29*(8), 695–708, doi:10.1134/1.1601648.
- Popov, N. A. (2009), Study of the formation and propagation of a leader channel in air, *Plasma Phys. Rep.*, *35*(9), 785–793, doi:10.1134/S1063780X09090074.
- Potter, D. (1973), *Computational Physics*, 304 pp., John Wiley, New York.
- Press, W. H., B. P. Flannery, S. A. Teukolsky, and W. T. Vetterling (1992), *Numerical Recipes in C: The Art of Scientific Computing*, 2nd ed., 1020 pp., Cambridge Univ. Press, Cambridge, U. K.
- Riousset, J. A., V. P. Pasko, P. R. Krehbiel, R. J. Thomas, and W. Rison (2007), Three-dimensional fractal modeling of intracloud lightning discharge in a New Mexico thunderstorm and comparison with lightning mapping observations, *J. Geophys. Res.*, *112*, D15203, doi:10.1029/2006JD007621.
- Riousset, J. A., V. P. Pasko, P. R. Krehbiel, W. Rison, and M. A. Stanley (2010), Modeling of thundercloud screening charges: Implications for blue and gigantic jets, *J. Geophys. Res.*, *115*, A00E10, doi:10.1029/2009JA014286.
- Sentman, D. D., H. C. Stenbaek-Nielsen, M. G. McHarg, and J. S. Morrill (2008a), Plasma chemistry of sprite streamers, *J. Geophys. Res.*, *113*, D11112, doi:10.1029/2007JD008941.
- Sentman, D. D., H. C. Stenbaek-Nielsen, M. G. McHarg, and J. S. Morrill (2008b), Correction to “Plasma chemistry of sprite streamers,” *J. Geophys. Res.*, *113*, D14399, doi:10.1029/2008JD010634.
- Stenbaek-Nielsen, H. C., M. G. McHarg, T. Kammae, and D. D. Sentman (2007), Observed emission rates in sprite streamer heads, *Geophys. Res. Lett.*, *34*, L11105, doi:10.1029/2007GL029881.
- Su, H. T., R. R. Hsu, A. B. Chen, Y. C. Wang, W. S. Hsiao, W. C. Lai, L. C. Lee, M. Sato, and H. Fukunishi (2003), Gigantic jets between a thundercloud and the ionosphere, *Nature*, *423*(6943), 974–976, doi:10.1038/nature01759.
- Tardiveau, P., E. Marode, A. Agneray, and M. Cheaib (2001), Pressure effects on the development of an electric discharge in non-uniform fields, *J. Phys. D Appl. Phys.*, *34*(11), 1690–1696.
- Taylor, R. L. (1974), Energy transfer processes in the stratosphere, *Can. J. Chem.*, *52*, 1436–1451.
- Vallance-Jones, A. V. (1974), *Aurora*, D. Reidel, Norwell, Mass.
- Vidal, F., et al. (2002), Modeling of the air plasma near the tip of the positive leader, *IEEE Trans. Plasma Sci.*, *30*(3), 1339–1349, doi:10.1109/TPS.2002.801538.
- Walter, C. W., P. C. Cosby, and H. Helm (1994), Predissociation quantum yields of singlet nitrogen, *Phys. Rev. A*, *50*(44), 2930–2936.
- Wescott, E. M., D. Sentman, H. C. Stenbaek-Nielsen, P. Huet, M. J. Heavner, and D. R. Moudry (2001), New evidence for the brightness and ionization of blue jets and blue starters, *J. Geophys. Res.*, *106*(A10), 21,549–21,554, doi:10.1029/2000JA000429.
- Zhao, X. M., J. C. Diels, C. Y. Wang, and J. M. Elizondo (1995), Femto-second ultraviolet laser pulse induced lightning discharge in gases, *IEEE J. Quantum Electron.*, *31*(3), 599–612.

A. Bourdon, Energetics and Combustion Laboratory, UPR CNRS 288, École Centrale Paris, Grande Voie des Vignes, F-92295 Châtenay-Malabry, France. (anne.bourdon@em2c.ecp.fr)

V. P. Pasko and J. A. Riousset, Communications and Space Sciences Laboratory, Department of Electrical Engineering, Pennsylvania State University, 211B Electrical Engineering East, University Park, PA 16802, USA. (rioussset@psu.edu; vpasko@psu.edu)